

Emergent chiral Higgs mode in π -flux frustrated lattices

M. Lanaro,^{1,2} L. Maffi,^{1,2} and M. Di Liberto^{1,2,3}

¹*Dipartimento di Fisica e Astronomia “G. Galilei”, Università degli Studi di Padova, I-35131, Padova, Italy*

²*INFN Istituto Nazionale di Fisica Nucleare, Sezione di Padova, I-35131, Padova, Italy*

³*Padua Quantum Technologies Research Center, via Marzolo 8, I-35131 Padova, Italy*

Neutral-atom quantum simulators provide a powerful platform for realizing strongly correlated phases, enabling access to dynamical signatures of quasiparticles and symmetry breaking processes. Motivated by recent observations of quantum phases in flux-frustrated ladders with non-vanishing ground state currents, we investigate interacting bosons on the dimerized BBH lattice in two dimensions—originally introduced in the context of higher-order topology. After mapping out the phase diagram, which includes vortex superfluid (V-SF), vortex Mott insulator (V-MI), and featureless Mott insulator (MI) phases, we focus on the integer filling case. There, the MI/V-SF transition simultaneously breaks the \mathbb{Z}_2^T and U(1) symmetries, where \mathbb{Z}_2^T corresponds to time-reversal symmetry (TRS). Using a slave-boson description, we resolve the excitation spectrum across the transition and uncover a chiral Higgs mode whose mass softens at criticality, providing a dynamical hallmark of emergent chirality that we numerically probe via quench dynamics. Our results establish an experimentally realistic setting for probing unconventional TRS-broken phases and quasiparticles with intrinsic chirality in strongly interacting quantum matter.

Introduction. Quantum simulation platforms based on neutral atoms are currently offering a versatile and tunable playground to access strongly-correlated phenomena in a variety of many-body models [1, 2]. Besides ground state properties, these platforms provide access to near-equilibrium dynamics and quenches, revealing non-trivial properties of the many-body spectra, even beyond computational capabilities. Monitoring out-of-equilibrium dynamics has allowed to identify the emergence of nontrivial quasiparticles, for example magnons in spin models [3, 4] or magnetic polarons in doped antiferromagnets [5, 6]. A prominent role in symmetry broken phases or near critical points of phase transitions is played by amplitude (Higgs) excitations [7], observed, for example, in interacting bosonic [8, 9] and fermionic systems [10, 11], long-range cavity systems [12], Rydberg spin systems [13] and predicted for dipolar supersolids [14]. Identifying unconventional quasiparticles in strongly-correlated quantum systems, including those appearing in lattice gauge theories [15, 16], is currently a major goal of quantum simulation platforms.

Programmable atomic analog devices have also successfully demonstrated the simulation of static and dynamical properties of charged particles in synthetic gauge fields [17–19], thus accessing states that break time-reversal symmetry (TRS). This direction, based on synthetic gauge potentials, is driven by the possibility of accessing topological states of matter like the Integer and Fractional Quantum Hall states [20]. While the former only requires the engineering of single-particle bands with non-zero Chern number, the latter cannot exist without interactions among the particles [21, 22], thus motivating their exploration with programmable quantum many-body systems. These states can display quasiparticle excitations that include Abelian and non-Abelian anyons

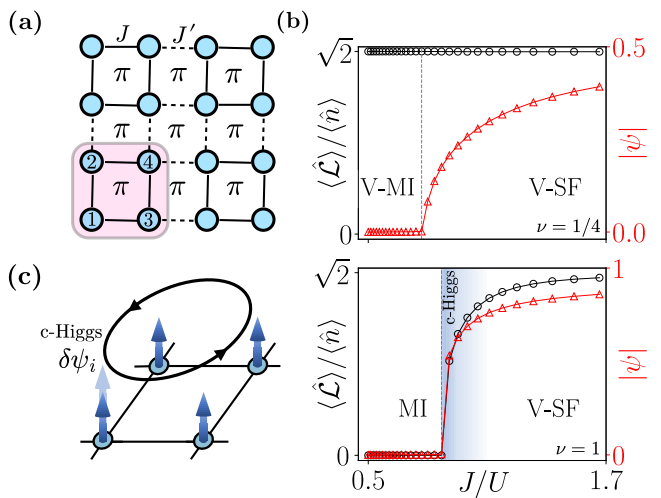


Figure 1. Model and main results. (a) Schematics of the BBH lattice with dimerized hopping J , J' and uniform π flux for interacting bosons. The unit cell is highlighted. (b) Ground-state loop current $\langle \hat{L} \rangle / \langle \hat{n} \rangle$ (black circles) and superfluid order parameter $|\psi|$ (red triangles) within cluster Gutzwiller approximation marking phase transitions between vortex superfluid (V-SF) and vortex Mott insulating (V-MI) phases for filling $\nu = 1/4$ (top) and between V-SF and Mott-insulating (MI) phases for $\nu = 1$ (bottom) for $J'/J = 0.03$. The region displaying a chiral Higgs excitation is highlighted. (c) Pictorial representation of chiral Higgs mode dynamics within a plaquette, where $\delta\psi_i$ indicates the amplitude excitation and the mode exhibits a finite loop current.

[23, 24] as well as chiral graviton-like modes [25, 26], thus stimulating efforts for their identification in synthetic matter systems [27, 28]. Recent progress in this direction has been demonstrated through the realization of Laughlin states with few atoms [29, 30]. To date, many-

body topologically ordered phases however remain still a challenge for analog quantum simulators, as compared to digital realizations [31].

Recent experimental advances in quasi-1D optical lattices geometries with fermions in synthetic dimensions [32] have shown the signature of a Hall response [33]. Bosonic ladder experiments [34, 35] have demonstrated the preparation of a Meissner phase [36], a strongly-interacting gapped phase with broken TRS. Such phase displays leg-currents that can be seen as precursor of FQHE edge modes in the sense of the wire construction [37, 38]. Key steps for its observation required the preparation of disconnected plaquette vortices, then adiabatically melted into each other. In this context, correlated quantum phases with ground states currents or vortices offer an intriguing quantum simulation scenario. Magnetic flux frustration and geometrical frustration can indeed give rise to a variety of quantum phases with broken TRS. Examples include Meissner or vortex phases, vortex Mott insulators, chiral superfluids, topological bosonic and Mott insulators [39–54], whose ground state properties and excitations are still to be observed. The recent experimental developments [35] suggest some of them to be within reach.

In this work, we examine interacting bosons on a flux-frustrated dimerized model, namely the time-reversal invariant BBH model with π -flux, see Fig. 1(a), recently introduced in the context of higher-order topological insulators [55, 56] and relevant to optical lattice experiments with dimerized lattices [35]. We identify vortex superfluid (V-SF), vortex Mott insulator (V-MI) and featureless Mott insulator (MI) phases via DMRG numerical simulations and a cluster Gutzwiller approach, Fig. 1(b). The MI/V-SF transition at integer filling in two dimensions simultaneously breaks the \mathbb{Z}_2^T and U(1) symmetries, where \mathbb{Z}_2^T indicates TRS. This is reflected in the excitation spectrum, where we identify a chiral Higgs mode carrying nonvanishing vorticity, Fig. 1(c), and softening at the critical point, as revealed by quench dynamics. Our results provide a pathway for investigating unexplored properties of strongly-correlated quantum matter, as for the emergence of unconventional quasiparticles with intrinsic chirality.

Model and quantum phases. We consider a system of softcore bosons on a dimerized lattice described in Fig. 1(a). This model displays a uniform π -flux and is thus described by the Benalcazar-Bernevig-Hughes (BBH) model [55, 56]. In this work, we consider the strongly dimerized limit $J \gg J'$, where J and J' describe the intra- and inter-plaquette couplings. The free particle Hamiltonian is thus $\hat{\mathcal{H}}_0 = \hat{\mathcal{H}}_J + \hat{\mathcal{H}}_{J'}$. Onsite interactions are described by $\hat{\mathcal{H}}_{\text{onsite}} = \frac{U}{2} \sum_p \sum_{i=1}^4 \hat{n}_{i,p} (\hat{n}_{i,p} - 1) - \mu \sum_p \sum_{i=1}^4 \hat{n}_{i,p}$, where p is a plaquette index, i a sublattice index according to the convention in Fig. 1(a), $U > 0$ the interaction strength and μ the chemical potential.

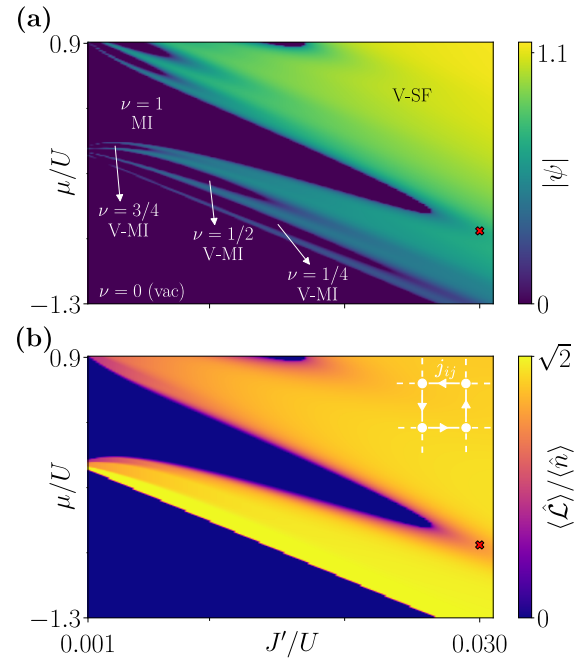


Figure 2. Phase diagram for $J'/J = 0.03$ of the 2D BBH model via cluster Gutzwiller approximation ($n_{\text{max}} = 5$). (a) Colormap of the superfluid order parameter $|\psi|$ showing Mott phase (MI), vortex Mott phases (V-MI) at different fillings and the vortex superfluid phase (V-SF). (b) Corresponding loop current per particle across the phase diagram. Notice that only the Mott lobe at $\nu = 1$ has zero loop current, while fractional fillings exhibit $\langle \hat{L} \rangle \neq 0$, indicating a V-MI phase. Inset shows the current pattern in V-SF and V-MI phases.

The model $\hat{\mathcal{H}} = \hat{\mathcal{H}}_0 + \hat{\mathcal{H}}_{\text{loc}}$ thus describes a BBH Bose-Hubbard model, which can be readily realized in optical superlattices via synthetic magnetic fields [35].

In the strongly dimerized limit each plaquette plays the role of a super-site. Here we perform our analysis using a cluster Gutzwiller ansatz (cGWA) [57–61], generalizing the more conventional single-site Gutzwiller ansatz [62, 63], allowing us to capture quantum phases at fractional filling as well as to retain quantum correlations within a plaquette [64]. Specifically we perform a decoupling by considering a plaquette product state of the form

$$|\Phi\rangle_{\text{cl}} \equiv \bigotimes_p \left(\sum_{n_1 n_2 n_3 n_4} c_{n_1 n_2 n_3 n_4}^{(p)} |n_1 n_2 n_3 n_4\rangle_p \right), \quad (1)$$

where p is the plaquette index and n_i denotes the Fock occupation number on the sublattice site i . Within this cluster mean-field decoupling, the Hamiltonian reads $\hat{\mathcal{H}} \approx \hat{\mathcal{H}}_{\text{cl}} - \sum_{\langle i,j \rangle} \left[J'_{ij} (\hat{b}_{i,p}^\dagger \psi^{j,q} - (\psi^{j,q})^* \psi^{i,p}) + \text{h.c.} \right]$ where

p, q are plaquettes indices, i, j are sublattice indices, $\psi^{i,p} \equiv \langle \hat{b}_{i,p} \rangle$ is the superfluid order parameter and $\hat{\mathcal{H}}_{\text{cl}}$ is the cluster Hamiltonian obtained by considering terms in $\hat{\mathcal{H}}$ that contain only operators acting on a single plaquette [65]. This allows us to write $\hat{\mathcal{H}} \approx \sum_p \hat{\mathcal{H}}_{\text{MF}}^{(p)}$,

where $\hat{\mathcal{H}}_{\text{MF}}^{(p)}$ contains only operators acting on a single plaquette p . We solve for the ground state by assuming (plaquette) translational symmetry for a two-dimensional (2D) lattice, namely $\psi^{i,p} = \psi^i$ and by diagonalizing $\hat{\mathcal{H}}_{\text{MF}}^{(p)}$ to find the cluster wavefunction parameters $c_{n_1 n_2 n_3 n_4}^{(p)}$ via a self-consistent algorithm (truncating $0 \leq n_i < n_{\text{max}}$ corresponding to a plaquette Hilbert space of dimension $d = n_{\text{max}}^4$). The resulting phase diagram is shown in Fig. 2(a).

In the strongly dimerized case, Ref. [52] showed that at low energies each plaquette p encodes two degenerate orbitals, $|\pm\rangle_p$, that are eigenstates of an emergent (plaquette) angular momentum operator $\hat{L}_z^{(p)}$ commuting with $\hat{\mathcal{H}}$, namely $\hat{L}_z^{(p)}|\pm\rangle_p = \pm|\pm\rangle_p$, and that carry (opposite) non-vanishing loop currents. At the plaquette level, interactions take the approximate form $\hat{\mathcal{H}}_{\text{onsite}} \propto -\sum_p [\hat{L}_z^{(p)}]^2 + \dots$ and favour the formation of ground state currents, $\hat{j}_{ij} = i(-J_{ij}\hat{b}_i^\dagger\hat{b}_j - \text{h.c.})$, maximizing the angular momentum and thus breaking TRS. The loop current operator within a plaquette, $\hat{\mathcal{L}}^{(p)} = \sum_{\square} \hat{j}_{ij} \approx \sqrt{2}\hat{L}_z^{(p)}$ with \sum_{\square} indicating the oriented sum within a plaquette, takes a non-zero expectation value. In the weakly-interacting limit, this corresponds to a macroscopic occupation of either $|+\rangle$ or $|-\rangle$, similarly to what happens in higher-band systems [66–70]. However, this feature persists in the strongly-correlated superfluid phase. The value of $\langle \hat{\mathcal{L}} \rangle$ across the phase diagram is shown in Fig. 2(b) and the corresponding phase is a V-SF that breaks $\mathbb{Z}_2^T \times \text{U}(1)$, with \mathbb{Z}_2^T indicating time-reversal symmetry. However, strong interactions lead to deviations from the low-energy theory where the loop current per particle, $\langle \hat{\mathcal{L}} \rangle / \langle \hat{n} \rangle$, is quantized in units of $\sqrt{2}$.

When interactions dominate, $U \gg J'$, different quantum phase transitions belonging to distinct universality classes occur depending on the filling ν (bosons per site). At filling $\nu = 1/2$, we confirm the transition identified via DMRG in Ref. [52] where the system enters a vortex Mott insulating phase (V-MI). The critical point belongs to the conventional O(2) universality class [71] as the symmetry breaking across the transition only involves U(1) symmetry. The system becomes incompressible and displays incoherent ground state currents. At filling $\nu = 1/4$, namely one particle per plaquette, we also find a V-MI phase. This is in contrast with what happens in p -band models, where the insulating phase corresponds to a staggered paramagnet with no orbital order [66, 69, 72]. To understand why the quantum fluctuations in our model still favour a V-MI phase we perform second order perturbation theory at $J'/U \ll 1$ for filling $\nu = 1/4$. For this, we consider the chiral basis introduced above, $|\pm\rangle$, representing the two chiral modes of a single particle in a π -flux plaquette via a spin-1/2. Perturbative calculations yield the quantum XXZ 2D Hamiltonian $\hat{H}_{\text{eff}} = -\frac{5}{2}\frac{J'^2}{U} - \frac{J'^2}{U} \sum_{\langle p,q \rangle} \left[\frac{3}{4}\hat{\sigma}_p^z\hat{\sigma}_q^z + \frac{1}{4}(\hat{\sigma}_p^x\hat{\sigma}_q^x + \hat{\sigma}_p^y\hat{\sigma}_q^y) \right]$.

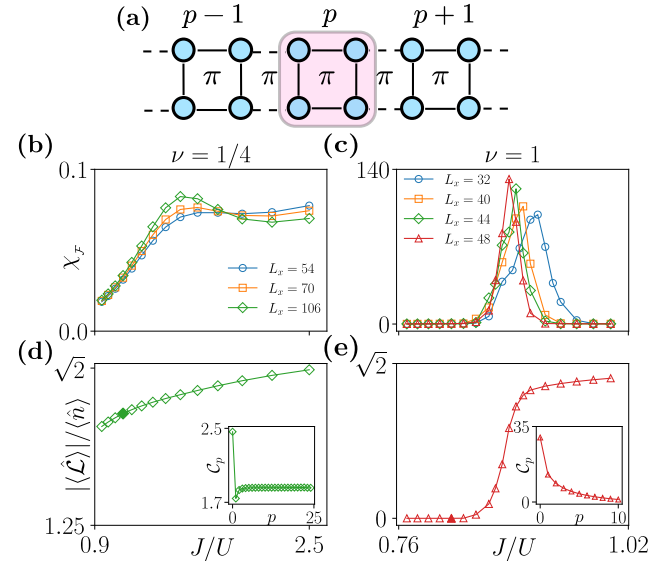


Figure 3. DMRG numerical results for a ladder with $J'/J = 0.1$. (a) Ladder geometry for DMRG simulations. (b)-(c) Fidelity susceptibilities χ_F for $\nu = 1/4$ and $\nu = 1$. The peaks growing with system size are indication of the phase transition. (d)-(e) Loop current per particle $|\langle \hat{\mathcal{L}} \rangle| / \langle \hat{n} \rangle$ for $L_x = 106$ ($\nu = 1/4$) and for $L_x = 48$ ($\nu = 1$). The $\nu = 1$ curve and the drop of loop current show the V-SF / MI phase transition. Insets show the \mathcal{C}_p correlator corresponding to the filled symbols.

Differently from p -band systems, where \hat{H}_{eff} is classical at leading order, we obtain a quantum effective model. Furthermore, the parameters in \hat{H}_{eff} put the ground state in the ferromagnetic phase [73], which corresponds to a V-MI phase for the model discussed here, as stated before. Finally, we also identified a transition to an insulating phase at $\nu = 3/4$ in a small regime of phase space.

At integer filling, $\nu = 1$, a completely different scenario takes place, which is the core of this work. Correlations within a plaquette will be suppressed when $U \gg J, J'$ and the system displays a transition onto a Mott insulating (MI) phase with a unique ground state, asymptotically connected to the product state $|1111\dots\rangle$. Differently from the previous cases, here the critical point belongs to a distinct universality class. In addition to U(1) (equivalently O(2)), the ground state also displays different time-reversal symmetry across the transition MI/V-SF, thus corresponding to the simultaneous breaking of $\mathbb{Z}_2^T \times \text{U}(1)$. This fact will have dramatic consequences in the excitation spectrum, as we will discuss down below.

DMRG analysis on a ladder. We complement our findings by performing DMRG simulations via the iTensor library [74] on a ladder of dimensions $L = 2 \times L_x$ shown in Fig. 3(a) for $J' = 0.1J$. We identify the transitions by computing the fidelity susceptibility, $\chi_F = -\left(\langle \psi(U +$

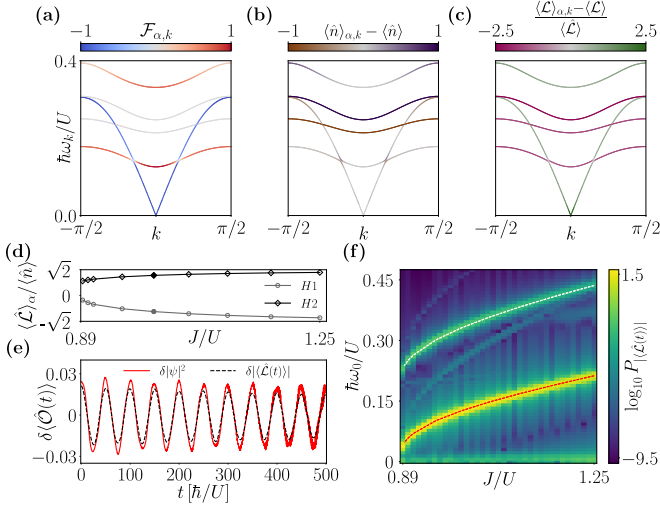


Figure 4. Low-energy excitations in the V-SF phase for filling $\nu = 1$. (a)-(c) Quasiparticle excitations for $|\mathbf{k}_x| = |\mathbf{k}_y| = k$, $J'/U = 0.03$, $J/U = 1.0$, and $\mu/U = -0.68$, corresponding to the cross symbols in Fig. 2. Spectra are colored based on the values of (a) flatness $\mathcal{F}_{\alpha,k}$, (b) plaquette density and (c) loop current $\langle \hat{L} \rangle_{\alpha,k}$. The index $\alpha = 1, \dots, 5$ labels the modes for increasing value of energy (d) Loop current per particle, $\langle \hat{L} \rangle_{\alpha} / \langle \hat{n} \rangle$ for H1 and H2. Filled symbols corresponds to spectra shown in the upper panel. (e) cGWA time evolution of loop current (black line) and local order parameter (red line) normalized to their ground-state values following a quench of a staggered flux $\pm\delta\theta$ per plaquette at unit filling. Parameters as in (a)-(c) and $\delta\theta = 0.01(J - \bar{J})/\bar{J}$ with $\bar{J} = 0.88U$. (f) Power spectrum of the loop current time evolution for different values J/U . Dashed lines highlight the frequencies corresponding to H1 (red) and H2 (white) modes.

$\delta U) |\psi(U)\rangle - 2 + \langle \psi(U - \delta U) |\psi(U)\rangle \big) / \delta U^2 L$, expected to diverge at the transition point [75]. We find two distinct peaks displayed in Fig. 3(b),(c): one occurs at $U/J \sim 0.65$ for $\nu = 1/4$ and another one at $U/J \sim 1.13$ for $\nu = 1$, whereas the transition at $\nu = 1/2$ was identified at $U/J \sim 1.2$ in Ref. [52]. The plaquette loop current $\langle \hat{L} \rangle$ manifests distinct behaviour for the two types of transitions, see Fig. 3(d),(e). While for $\nu = 1/4$ the loop current remains finite and smooth across the critical point, for $\nu = 1$ we observe a clear drop signaling that the ground state restores time-reversal symmetry in the insulating phase. In the insets, we estimate the loop current correlations between plaquettes, $\mathcal{C}_p = \langle \hat{L}_0 \hat{L}_p \rangle$, showing that the $\nu = 1/4$ insulating phase displays ferromagnetic long-range order as predicted by the perturbative analysis discussed above; instead, for $\nu = 1$, \mathcal{C}_p decays exponentially as expected in a featureless MI phase. The identification of the transition at filling $\nu = 3/4$ with DMRG has instead proven to be computationally challenging, as already anticipated by the narrow parameters range predicted by the cGWA phase diagram.

Excitations near the critical point. Quantum phase

transitions belonging to distinct universality classes are expected to display low-energy excitations of different nature [76]. The fractional filling critical points are in the O(2) universality class as the only symmetry broken across the transition is U(1), like in conventional Mott-superfluid transitions [7, 71, 76]. In this case, besides a low-energy gapless Goldstone mode, an amplitude (Higgs) excitation softens, as it was experimentally confirmed [8, 9]. At integer filling, the ground state additionally breaks TRS across the critical point and novel modes thus appear.

To describe the low-energy excitation spectra, we extend the slave boson approach described in Ref. [77] to the cluster formalism used in this work. This and similar approaches [78–80] have proven to accurately capture the excitations gaps observed experimentally [9] and can include quantum fluctuations in a controlled manner [77, 81]. Within this framework, for each plaquette we introduce slave boson operators $\hat{\beta}_{p,\mathbf{n}}$, spanning the plaquette Hilbert space $|n_1 n_2 n_3 n_4\rangle_p \equiv |\mathbf{n}\rangle_p = \hat{\beta}_{p,\mathbf{n}}^\dagger |0_{SB}\rangle$, where $|0_{SB}\rangle$ is a fictitious slave boson vacuum and $\sum_{\mathbf{n}} \hat{\beta}_{p,\mathbf{n}}^\dagger \hat{\beta}_{p,\mathbf{n}} = 1$. The diagonalization of the cluster mean-field Hamiltonian $\hat{\mathcal{H}}_{\text{MF}}^{(p)}$ provides a set of plaquette normal modes described by the unitary transformation $U_{m,\mathbf{n}}^{(p)}$ that we use to rotate the slave boson operators into via the linear transformation $\hat{\gamma}_{p,m}^\dagger = \sum_{\mathbf{n}} U_{m,\mathbf{n}}^{(p)} \hat{\beta}_{p,\mathbf{n}}^\dagger$, where m labels each plaquette normal mode with increasing energy. The bosonic creation operator can then be expressed as $\hat{b}_{i,p}^\dagger = \sum_{\mathbf{n}\mathbf{n}'} \langle \mathbf{n} | \hat{\beta}_{i,p}^\dagger | \mathbf{n}' \rangle \hat{\beta}_{p,\mathbf{n}}^\dagger \hat{\beta}_{p,\mathbf{n}'} = \sum_{n,m} \hat{\gamma}_{p,n}^\dagger \hat{F}_{nm}^{i,p} \hat{\gamma}_{p,m}$. Within the slave boson approach, we approximate $\hat{\mathcal{H}}_{\text{MF}}^{(p)}$ by condensing $\hat{\gamma}_{p,m=0}^{(\dagger)} \approx 1$ and by treating $\hat{\gamma}_{p,m \neq 0}^{(\dagger)}$ as weak quantum fluctuations up to quadratic order. In momentum space, we obtain the quadratic Hamiltonian $\hat{\mathcal{H}} \approx \hat{\mathcal{H}}^{(2)} = \frac{1}{2} \sum_{\mathbf{k}} (\hat{\gamma}_{\mathbf{k}}^\dagger, \hat{\gamma}_{-\mathbf{k}}) H_{\mathbf{k}} (\hat{\gamma}_{\mathbf{k}}, \hat{\gamma}_{-\mathbf{k}})^T$, where $\hat{\gamma}_p = 1/\sqrt{N} \sum_{\mathbf{k}} e^{i\mathbf{k} \cdot \mathbf{r}_p} \hat{\gamma}_{\mathbf{k}}$, $\hat{\gamma}_p = (\hat{\gamma}_{p,1}, \dots, \hat{\gamma}_{p,n} \dots \hat{\gamma}_{p,d})^T$ [65] and $H_{\mathbf{k}}$ is a $(2d-2) \times (2d-2)$ BdG Hamiltonian matrix. As shown in Fig. 4(a)-(c) near the critical point of the transition at $\nu = 1$, the excitation spectra obtained from $H_{\mathbf{k}}$ display several low-energy branches in the superfluid phase. The gapless branch corresponds to the Goldstone (phase) mode. However, other low-energy gapped modes appear. The analysis of the phase and amplitude character of the order parameter, obtained via the flatness $\mathcal{F}_{\alpha,\mathbf{k}}$ [9, 80], reveals that two of the gapped excitations (H1 and H2) are amplitude (Higgs) modes with $\mathcal{F}_{\alpha,\mathbf{k}} \approx 1$ and only one softening at the transition, see Fig. 4(d), whereas only the lowest mode is a phase (Goldstone) mode ($\mathcal{F}_{\alpha,\mathbf{k}} \approx -1$). This result is in contrast to the more conventional behavior of Mott-superfluid transitions with only a single Higgs excitation. Two other dispersive modes appear with neither amplitude nor phase character. As shown in Fig. 4(b), these modes are particle or hole excitations as indicated by computing

the density variation carried by each of them and their particle-hole character, see Ref. [80]. The chiral nature of the excitations can be revealed by estimating the loop current for each branch, as shown in Fig. 4(c). The two Higgs modes both carry a finite loop current and far away from the critical point its value tends to the effective theory prediction $|\langle \hat{\mathcal{L}} \rangle| \rightarrow \sqrt{2}$ in the deep superfluid regime [52]. However, the lowest-energy Higgs mode (H1) exhibits a loop current of opposite sign as compared to the ground state one, thus manifesting a chiral nature. This hierarchy is a consequence of the fact that the insulating phase does not break TRS, and the lowest Higgs mode is there to carry away the ground state loop current across the transition. Notice that this multi-Higgs structure only appears near the $\nu = 1$ critical point, whereas at fractional fillings a more conventional picture with a single Higgs mode occurs [65].

In order to probe the lowest Higgs chiral mode H1, we perform a quench by adding a weak staggered flux perturbation $\pm\delta\theta$ [18], which preserves U(1) and explicitly breaks TRS. As shown in Fig. 4(e), this selectively excites coherent oscillations of loop current and order parameter. A Fourier spectral analysis, Fig. 4(f), reveals a dominant peak corresponding to the chiral Higgs mode H1, negligible excitation of H2 and no particle (hole) weight, consistent with the fact that the quench preserves the global U(1) symmetry [9, 82].

Discussion and conclusions. In this work we have shown that interacting bosons on a dimerized flux-frustrated lattice display distinct quantum phases that spontaneously break TRS manifesting in vortex Mott and superfluid phases. The transition at integer filling breaks TRS and U(1) symmetries, with an excitation spectrum consisting of Higgs quasiparticles, including a chiral one. Our results provide an example of a strongly-correlated system with nontrivial quasi particles that is especially relevant in the context of very recent experimental developments employing dimerized lattices with synthetic gauge fields [35] and the corresponding direct measurement of the current patterns. Our work opens several questions concerning, for example, the decay and lifetime of the quasiparticles here identified [82] or the critical properties of the $\nu = 1$ transition [76]. Further investigations are needed to elucidate the interplay between topology and interactions in the BBH model at different fillings [83, 84], as for the SSH case [85], the possibility to stabilize topological phases via interactions [86]. In addition, it would be interesting to explore effects beyond strong dimerization that are not captured by our analysis and the role played by gauge symmetries [87] and chiral bound pairs [88] in transport phenomena. Our work paves the way to the identification of other unconventional critical points in chiral systems [45], including those connected to deconfined critical points [39, 89, 90].

Acknowledgements. The authors thank N. Gold-

man, M. Morgavi, S. Montangero and L. Pavešić for fruitful discussions. This work has received funding under the Horizon Europe programme HORIZON-CL4-2022-QUANTUM-02-SGA via the project 101113690 (PASQuanS2.1) and has been supported by the INFN project Iniziativa Specifica IS-Quantum, the Italian Ministry of University and Research via the Excellence grant 2023-2027 “Quantum Frontiers”, the Rita Levi-Montalcini program. The authors also acknowledge computational resources by Cloud Veneto.

- [1] I. M. Georgescu, S. Ashhab, and F. Nori, *Rev. Mod. Phys.* **86**, 153 (2014).
- [2] C. Gross and I. Bloch, *Science* **357**, 995 (2017).
- [3] T. Fukuhara, P. Schauß, M. Endres, S. Hild, M. Cheneau, I. Bloch, and C. Gross, *Nature* **502**, 76 (2013).
- [4] C. Chen, G. Emperauger, G. Bornet, F. Caleca, B. Gély, M. Bintz, S. Chatterjee, V. Liu, D. Barredo, N. Y. Yao, T. Lahaye, F. Mezzacapo, T. Roscilde, and A. Browaeys, *Science* **389**, 483 (2025).
- [5] J. Koepsell, J. Vijayan, P. Sompét, F. Grusdt, T. A. Hilker, E. Demler, G. Salomon, I. Bloch, and C. Gross, *Nature* **572**, 358 (2019).
- [6] M. L. Prichard, Z. Ba, I. Morera, B. M. Spar, D. A. Huse, E. Demler, and W. S. Bakr, *Nature Physics* , 1 (2025).
- [7] D. Pekker and C. Varma, *Annu. Rev. Condens. Matter Phys.* **6**, 269 (2015).
- [8] U. Bissbort, S. Götze, Y. Li, J. Heinze, J. S. Krauser, M. Weinberg, C. Becker, K. Sengstock, and W. Hofstetter, *Physical Review Letters* **106**, 205303 (2011).
- [9] M. Endres, T. Fukuhara, D. Pekker, M. Cheneau, P. Schauß, C. Gross, E. Demler, S. Kuhr, and I. Bloch, *Nature* **487**, 454 (2012).
- [10] A. Behrle, T. Harrison, J. Kombe, K. Gao, M. Link, J.-S. Bernier, C. Kollath, and M. Köhl, *Nature Physics* **14**, 781 (2018).
- [11] A. Kell, M. Breyer, D. Eberz, and M. Köhl, *Phys. Rev. Lett.* **133**, 150403 (2024).
- [12] J. Léonard, A. Morales, P. Zupancic, T. Donner, and T. Esslinger, *Science* **358**, 1415 (2017).
- [13] T. Manovitz, S. H. Li, S. Ebadi, R. Samajdar, A. A. Geim, S. J. Evered, D. Bluvstein, H. Zhou, N. U. Koyluoglu, J. Feldmeier, *et al.*, *Nature* **638**, 86 (2025).
- [14] J. Hertkorn, F. Böttcher, M. Guo, J. N. Schmidt, T. Langen, H. P. Büchler, and T. Pfau, *Phys. Rev. Lett.* **123**, 193002 (2019).
- [15] M. Aidelsburger, L. Barbiero, A. Bermudez, T. Chanda, A. Dauphin, D. González-Cuadra, P. R. Grzybowski, S. Hands, F. Jendrzejewski, J. Jünemann, *et al.*, *Philosophical Transactions of the Royal Society A: Mathematical, Physical and Engineering Sciences* **380** (2022).
- [16] J. C. Halimeh, M. Aidelsburger, F. Grusdt, P. Hauke, and B. Yang, *Nature Physics* **21**, 25 (2025).
- [17] D. Jaksch and P. Zoller, *New Journal of Physics* **5**, 56 (2003).
- [18] M. Aidelsburger, M. Atala, S. Nascimbène, S. Trotzky, Y.-A. Chen, and I. Bloch, *Phys. Rev. Lett.* **107**, 255301 (2011).
- [19] N. Goldman, J. C. Budich, and P. Zoller, *Nature Physics*

12, 639 (2016).

[20] N. Cooper, J. Dalibard, and I. Spielman, *Reviews of modern physics* **91**, 015005 (2019).

[21] R. B. Laughlin, *Physical Review Letters* **50**, 1395 (1983).

[22] R. E. Prange and S. M. Girvin, *The quantum Hall effect* (Springer, 1987).

[23] B. I. Halperin, *Physical Review Letters* **52**, 1583 (1984).

[24] A. Stern, *Annals of Physics* **323**, 204 (2008).

[25] F. Haldane, *Physical review letters* **107**, 116801 (2011).

[26] J. Liang, Z. Liu, Z. Yang, Y. Huang, U. Wurstbauer, C. R. Dean, K. W. West, L. N. Pfeiffer, L. Du, and A. Pinczuk, *Nature* **628**, 78 (2024).

[27] Z. Bacciconi, H. B. Xavier, I. Carusotto, T. Chanda, and M. Dalmonte, *Physical Review X* **15**, 021027 (2025).

[28] H. B. Xavier, Z. Bacciconi, T. Chanda, D. T. Son, and M. Dalmonte, *Physical Review Letters* **135**, 196501 (2025).

[29] J. Léonard, S. Kim, J. Kwan, P. Segura, F. Grusdt, C. Repellin, N. Goldman, and M. Greiner, *Nature* **619**, 495 (2023).

[30] P. Lunt, P. Hill, J. Reiter, P. M. Preiss, M. Galka, and S. Jochim, *Physical Review Letters* **133**, 253401 (2024).

[31] S. J. Evered, M. Kalinowski, A. A. Geim, T. Manovitz, D. Bluvstein, S. H. Li, N. Maskara, H. Zhou, S. Ebadi, M. Xu, *et al.*, *Nature* **645**, 341 (2025).

[32] T.-W. Zhou, G. Cappellini, D. Tusi, L. Franchi, J. Paravicini, C. Repellin, S. Greschner, M. Inguscio, T. Giamarchi, M. Filippone, *et al.*, *Science* **381**, 427 (2023).

[33] S. Greschner, M. Filippone, and T. Giamarchi, *Phys. Rev. Lett.* **122**, 083402 (2019).

[34] M. Atala, M. Aidelsburger, M. Lohse, J. T. Barreiro, B. Paredes, and I. Bloch, *Nature Physics* **10**, 588 (2014).

[35] A. Impertro, S. Huh, S. Karch, J. F. Wienand, I. Bloch, and M. Aidelsburger, *Nature Physics* , 1 (2025).

[36] E. Orignac and T. Giamarchi, *Phys. Rev. B* **64**, 144515 (2001).

[37] C. L. Kane, R. Mukhopadhyay, and T. C. Lubensky, *Phys. Rev. Lett.* **88**, 036401 (2002).

[38] M. Calvanese Strinati, E. Cornfeld, D. Rossini, S. Barbarino, M. Dalmonte, R. Fazio, E. Sela, and L. Mazza, *Phys. Rev. X* **7**, 021033 (2017).

[39] M. Polini, R. Fazio, A. H. MacDonald, and M. P. Tosi, *Phys. Rev. Lett.* **95**, 010401 (2005).

[40] L.-K. Lim, C. M. Smith, and A. Hemmerich, *Phys. Rev. Lett.* **100**, 130402 (2008).

[41] M.-C. Cha and J.-G. Shin, *Phys. Rev. A* **83**, 055602 (2011).

[42] A. Dhar, T. Mishra, M. Maji, R. V. Pai, S. Mukerjee, and A. Paramekanti, *Phys. Rev. B* **87**, 174501 (2013).

[43] A. Dauphin, M. Müller, and M. A. Martin-Delgado, *Phys. Rev. A* **86**, 053618 (2012).

[44] S. Greschner, L. Santos, and T. Vekua, *Phys. Rev. A* **87**, 033609 (2013).

[45] M. P. Zaletel, S. A. Parameswaran, A. Rüegg, and E. Altman, *Phys. Rev. B* **89**, 155142 (2014).

[46] F. Kolley, M. Piraud, I. P. McCulloch, U. Schollwöck, and F. Heidrich-Meisner, *New Journal of Physics* **17**, 092001 (2015).

[47] M. Piraud, F. Heidrich-Meisner, I. P. McCulloch, S. Greschner, T. Vekua, and U. Schollwöck, *Phys. Rev. B* **91**, 140406 (2015).

[48] S. Greschner, M. Piraud, F. Heidrich-Meisner, I. P. McCulloch, U. Schollwöck, and T. Vekua, *Phys. Rev. Lett.* **115**, 190402 (2015).

[49] M. Piraud, F. Heidrich-Meisner, I. P. McCulloch, S. Greschner, T. Vekua, and U. Schollwöck, *Phys. Rev. B* **91**, 140406 (2015).

[50] S. Greschner, M. Piraud, F. Heidrich-Meisner, I. P. McCulloch, U. Schollwöck, and T. Vekua, *Phys. Rev. A* **94**, 063628 (2016).

[51] C.-M. Halati and T. Giamarchi, *Phys. Rev. Res.* **5**, 013126 (2023).

[52] M. Di Liberto and N. Goldman, *Phys. Rev. Res.* **5**, 023064 (2023).

[53] L. Barbiero, J. Cabedo, M. Lewenstein, L. Tarruell, and A. Celi, *Phys. Rev. Res.* **5**, L042008 (2023).

[54] A. Dasgupta, M. Lacki, H. Korbacher, G. A. Domínguez-Castro, J. Zakrzewski, and L. Santos, *arXiv preprint arXiv:2511.07042* (2025).

[55] W. A. Benalcazar, B. A. Bernevig, and T. L. Hughes, *Science* **357**, 61 (2017).

[56] W. A. Benalcazar, B. A. Bernevig, and T. L. Hughes, *Phys. Rev. B* **96**, 245115 (2017).

[57] D.-S. Lühmann, *Phys. Rev. A* **87**, 043619 (2013).

[58] D. Yamamoto, A. Masaki, and I. Danshita, *Phys. Rev. B* **86**, 054516 (2012).

[59] D. Huerga, J. Dukelsky, and G. E. Scuseria, *Phys. Rev. Lett.* **111**, 045701 (2013).

[60] D. Yamamoto, G. Marmorini, and I. Danshita, *Phys. Rev. Lett.* **112**, 127203 (2014).

[61] G. C. Paul, P. Recher, and L. Santos, *arXiv preprint arXiv:2507.12153* (2025).

[62] W. Krauth, M. Caffarel, and J.-P. Bouchaud, *Phys. Rev. B* **45**, 3137 (1992).

[63] D. Jaksch, C. Bruder, J. I. Cirac, C. W. Gardiner, and P. Zoller, *Phys. Rev. Lett.* **81**, 3108 (1998).

[64] A single-site ansatz is described by a wavefunction $|\psi_i\rangle = \sum_n c_n |n\rangle$. Using such ansatz, the fractional filling condition, *e.g.* $\langle \hat{n}_i \rangle = 1/2$, necessarily implies $\langle \hat{b}_i \rangle \neq 0$. This forbids the possibility to capture phase transitions into insulating phases with fractional filling within a single-site Gutzwiller ansatz.

[65] See Supplemental Material.

[66] A. Isacsson and S. M. Girvin, *Phys. Rev. A* **72**, 053604 (2005).

[67] W. V. Liu and C. Wu, *Phys. Rev. A* **74**, 013607 (2006).

[68] G. Wirth, M. Ölschläger, and A. Hemmerich, *Nature Physics* **7**, 147 (2011).

[69] X. Li and W. V. Liu, *Reports on Progress in Physics* **79**, 116401 (2016).

[70] X. Li, Z. Zhang, and W. V. Liu, *Phys. Rev. Lett.* **108**, 175302 (2012).

[71] E. Altman and A. Auerbach, *Phys. Rev. Lett.* **89**, 250404 (2002).

[72] X. Li, E. Zhao, and W. V. Liu, *Phys. Rev. A* **83**, 063626 (2011).

[73] D. Peter, S. Müller, S. Wessel, and H. P. Büchler, *Phys. Rev. Lett.* **109**, 025303 (2012).

[74] M. Fishman, S. R. White, and E. M. Stoudenmire, *SciPost Phys. Codebases* , 4 (2022).

[75] J. Carrasquilla, S. R. Manmana, and M. Rigol, *Phys. Rev. A* **87**, 043606 (2013).

[76] S. Sachdev, *Quantum phases of matter* (Cambridge University Press, 2023).

[77] I. Frérot and T. Roscilde, *Phys. Rev. Lett.* **116**, 190401 (2016).

[78] S. D. Huber, E. Altman, H. P. Büchler, and G. Blatter,

Phys. Rev. B **75**, 085106 (2007).

[79] K. V. Krutitsky, *Physics Reports* **607**, 1 (2016).

[80] M. Di Liberto, A. Recati, N. Trivedi, I. Carusotto, and C. Menotti, *Phys. Rev. Lett.* **120**, 073201 (2018).

[81] F. Caleffi, M. Capone, C. Menotti, I. Carusotto, and A. Recati, *Phys. Rev. Res.* **2**, 033276 (2020).

[82] D. Podolsky, A. Auerbach, and D. P. Arovas, *Phys. Rev. B* **84**, 174522 (2011).

[83] J. Bibo, I. Lovas, Y. You, F. Grusdt, and F. Pollmann, *Phys. Rev. B* **102**, 041126 (2020).

[84] D. González-Cuadra, *Phys. Rev. B* **105**, L020403 (2022).

[85] F. Grusdt, M. Höning, and M. Fleischhauer, *Phys. Rev. Lett.* **110**, 260405 (2013).

[86] H. Kamal, J. Kemp, Y.-C. He, Y. Fuji, M. Aidelsburger, P. Zoller, and N. Y. Yao, *Phys. Rev. Lett.* **133**, 163403 (2024).

[87] M. Burgher, M. Di Liberto, N. Goldman, and I. Amelio, *Phys. Rev. B* **111**, 064514 (2025).

[88] A. A. Stepanenko and M. Di Liberto, *Phys. Rev. A* **110**, L061304 (2024).

[89] T. Senthil, A. Vishwanath, L. Balents, S. Sachdev, and M. P. Fisher, *Science* **303**, 1490 (2004).

[90] T. Senthil, 50 Years of the Renormalization Group: Dedicated to the Memory of Michael E Fisher , 169 (2024).

Supplemental Material

CLUSTER MEAN-FIELD APPROXIMATION.

The Hamiltonian of our 2D system can be written as $\hat{\mathcal{H}} = \hat{\mathcal{H}}_J + \hat{\mathcal{H}}_{\text{onsite}} + \hat{\mathcal{H}}_{J'}$, where

$$\begin{aligned}\hat{\mathcal{H}}_J &= -J \sum_p \left(e^{i\pi} \hat{b}_{1,p}^\dagger \hat{b}_{2,p} + \hat{b}_{2,p}^\dagger \hat{b}_{4,p} + \hat{b}_{4,p}^\dagger \hat{b}_{3,p} + \hat{b}_{3,p}^\dagger \hat{b}_{1,p} + \text{h.c.} \right), \\ \hat{\mathcal{H}}_{J'} &= -J' \sum_p \left(e^{i\pi} \hat{b}_{2,p}^\dagger \hat{b}_{1,p+\hat{\mathbf{u}}_y} + \hat{b}_{4,p}^\dagger \hat{b}_{3,p+\hat{\mathbf{u}}_y} + \hat{b}_{4,p}^\dagger \hat{b}_{2,p+\hat{\mathbf{u}}_x} + \hat{b}_{3,p}^\dagger \hat{b}_{1,p+\hat{\mathbf{u}}_x} + \text{h.c.} \right), \\ \hat{\mathcal{H}}_{\text{onsite}} &= \frac{U}{2} \sum_p \sum_{i=1}^4 \hat{n}_{i,p} (\hat{n}_{i,p} - 1) - \mu \sum_p \sum_{i=1}^4 \hat{n}_{i,p},\end{aligned}\tag{S1}$$

where $(\hat{\mathbf{u}}_x, \hat{\mathbf{u}}_y)$ are unit vectors along the x and y directions. We solve the Hamiltonian $\hat{\mathcal{H}}$ within a cluster Gutzwiller ansatz approximation, namely a mean-field ansatz for plaquettes,

$$|\Phi\rangle_{\text{cl}} \equiv \bigotimes_p \left(\sum_{n_1 n_2 n_3 n_4} c_{n_1 n_2 n_3 n_4}^{(p)} |n_1 n_2 n_3 n_4\rangle_p \right),\tag{S2}$$

from which we can rewrite $\hat{\mathcal{H}}$ as

$$\hat{\mathcal{H}} \approx \hat{\mathcal{H}}_{\text{cl}} + \hat{\mathcal{H}}',\tag{S3}$$

with $\hat{\mathcal{H}}_{\text{cl}} = \hat{\mathcal{H}}_J + \hat{\mathcal{H}}_{\text{onsite}}$ and the coupling between different plaquettes taking the form

$$\hat{\mathcal{H}}_{J'} \rightarrow \hat{\mathcal{H}}' = - \sum_{\substack{\langle p,q \rangle \\ \langle i,j \rangle}} \left[J'_{ij} \left(\hat{b}_{i,p}^\dagger \psi^{j,q} - (\psi^{j,q})^* \psi^{i,p} \right) + \text{h.c.} \right],\tag{S4}$$

where $\psi^{i,p} \equiv \langle \hat{b}_{i,p} \rangle$ is the order parameter for the i -th site of the p -th plaquette. This allows us to write $\hat{\mathcal{H}} \approx \sum_p \hat{\mathcal{H}}_{\text{MF}}^{(p)}$, where $\hat{\mathcal{H}}_{\text{MF}}^{(p)}$ contains only operators acting on a single plaquette p . The local basis here takes the form $|\mathbf{n}\rangle = |n_1 n_2 n_3 n_4\rangle$, where the different $(n_1, n_2, n_3, n_4) \equiv \mathbf{n}$ represent the occupation number on each site of the sublattice of the plaquette. We truncate to $n_i < n_{\text{max}}$, with $n_{\text{max}} = 5$ and a corresponding local Hilbert space dimension $d = n_{\text{max}}^4$. The Fock states are generated by a fictitious slave boson vacuum, $|\mathbf{n}\rangle_p = \hat{\beta}_{p,\mathbf{n}}^\dagger |0_{SB}\rangle_p$, with $\sum_{\mathbf{n}} \hat{\beta}_{p,\mathbf{n}}^\dagger \hat{\beta}_{p,\mathbf{n}} = 1$. We rotate this $\hat{\beta}$ operators to new $\hat{\gamma}$ operators via

$$\hat{\gamma}_{p,n}^\dagger = \sum_{\mathbf{n}} U_{n,\mathbf{n}}^{(p)} \hat{\beta}_{p,\mathbf{n}}^\dagger,\tag{S5}$$

with $U_{n,\mathbf{n}}^{(p)}$ the unitary transformation that diagonalizes the mean-field solution of $\hat{\mathcal{H}}$, namely $\hat{\mathcal{H}}_{\text{MF}}^{(p)}$, and whose columns are the mean-field eigenvectors $\Psi^{(p)} = (\psi_0^{(p)}, \dots, \psi_n^{(p)}, \dots, \psi_d^{(p)})$

$$\langle \mathbf{n} | \Psi_n^{(p)} \rangle = U_{n,\mathbf{n}}^{(p)}.\tag{S6}$$

In this way, we get a Hamiltonian with quartic terms in $\hat{\gamma}$ for the hopping part $\hat{\mathcal{H}}_{J'}$, and quadratic terms (within the plaquette) for the rest. In terms of the rotated $\hat{\gamma}$ operators, the Hamiltonian takes the form

$$\hat{\mathcal{H}} = -J' \sum_{\langle p,q \rangle} \sum_{\langle i,j \rangle} \left(\hat{\gamma}_p^\dagger \tilde{F}^{i,p} \hat{\gamma}_p \hat{\gamma}_q^\dagger [\tilde{F}^{j,q}]^\dagger \hat{\gamma}_q + \text{h.c.} \right) + \sum_p \hat{\gamma}_p^\dagger \tilde{G} \hat{\gamma}_p,\tag{S7}$$

where

$$\hat{\gamma}_{p,n}^\dagger = \sum_{\mathbf{n}} \langle \mathbf{n} | \Psi_n^{(p)} \rangle \hat{\beta}_{p,\mathbf{n}}^\dagger,\tag{S8}$$

$$\hat{\gamma}_p = (\hat{\gamma}_{p,0}, \dots, \hat{\gamma}_{p,n}, \dots, \hat{\gamma}_{p,d})^T,\tag{S9}$$

$$\tilde{F}_{nm}^{i,p} = \langle \Psi_n^{(p)} | \hat{b}_{i,p}^\dagger | \Psi_m^{(p)} \rangle,\tag{S10}$$

$$\tilde{G}_{nm} = \langle \Psi_n^{(p)} | \hat{\mathcal{H}}_J + \hat{\mathcal{H}}_{\text{onsite}} | \Psi_m^{(p)} \rangle.\tag{S11}$$

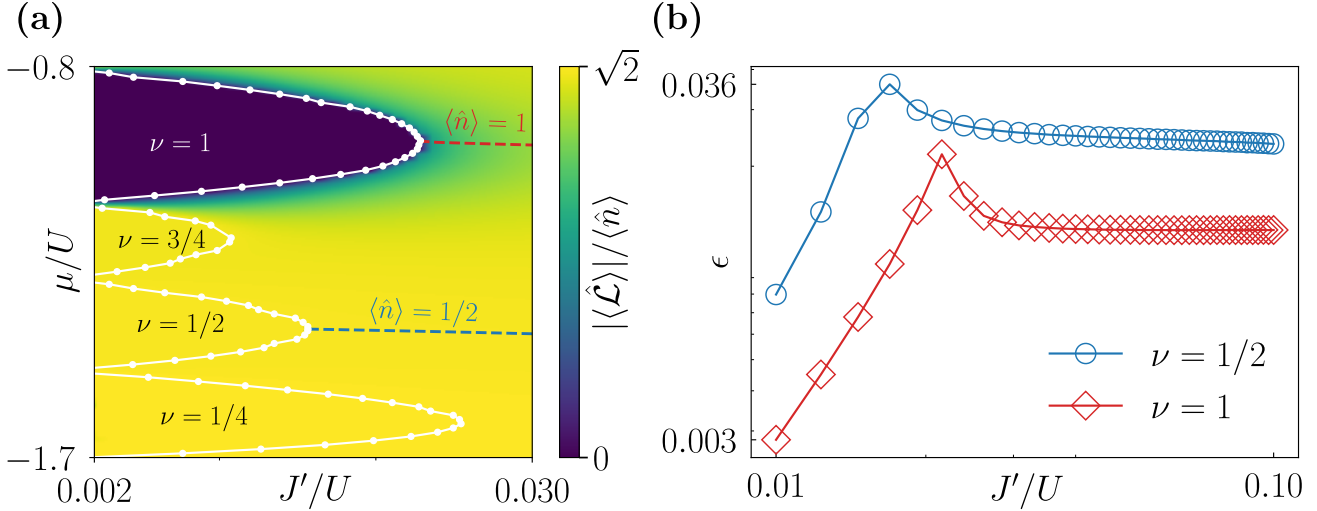


Figure S1. (a) Phase diagram along the cut at fixed $J/U = 1.2$. White dots mark the transition points from the V-SF (right) to the (V)-MI (left), while the dotted curves shows the constant filling lines for $\nu = 1$ (red) and $\nu = 1/2$ (blue). The vertical axis shows the ground-state loop current. The lobe at integer filling exhibits zero loop current, while the fractional-filling lobes correspond to V-MI phases with finite current. (b) Control parameter at integer (red) and half (blue) filling for $J/U = 1.2$ as a function of J'/U . The control parameter displays a peak at the transition point and remains below $\epsilon \sim 0.04$.

Notice that in the definition of \tilde{G}_{nm} we have included also hopping processes within the plaquette, which marks a difference with the treatment discussed in Ref. [77] and allows us to introduce intra-plaquette correlations. In order to proceed further with the calculations we perform now a quadratic approximation around the mean field minimum, condensing the $\hat{\gamma}_{p,0}$ bosons ($\hat{\gamma}_{p,0}^\dagger \approx 1$) and treating the other bosonic fields as perturbations, i.e. $\hat{\gamma}_{p,n \neq 0}^\dagger \hat{\gamma}_{p,n \neq 0} \ll 1$. In this way (Bogoliubov shift)

$$\hat{\gamma}_{p,0}^{(\dagger)} \approx \sqrt{1 - \sum_{n \neq 0} \hat{\gamma}_{p,n}^\dagger \hat{\gamma}_{p,n}} \approx 1 - \frac{1}{2} \sum_{n \neq 0} \hat{\gamma}_{p,n}^\dagger \hat{\gamma}_{p,n} + O(\hat{\gamma}^4). \quad (\text{S12})$$

In order for this to be consistent, we must verify that the average values of the non-condensed slave bosons remains small in the renormalized ground state, i.e.

$$\epsilon = \sum_{n>0} \langle \hat{\gamma}_{p,n}^\dagger \hat{\gamma}_{p,n} \rangle \ll 1, \quad (\text{S13})$$

as we can see in Fig. S1(b) for the cut with fixed $J/U = 1.2$ (phase diagram shown in Fig. S1(a)). In this figure, the peak in the control parameter appears at the critical point for filling $\nu = 1$ and $\nu = 1/2$, but we can observe how ϵ remains always small. With this, the field operator $\hat{b}_{i,p}^\dagger$ is expressed as

$$\begin{aligned} \hat{b}_{i,p}^\dagger &= \sum_{nm} \hat{\gamma}_{p,n}^\dagger \tilde{F}_{nm}^{i,p} \hat{\gamma}_{p,m} \\ &= \hat{\gamma}_{p,0}^\dagger \tilde{F}_{00}^{i,p} \hat{\gamma}_{p,0} + \sum_{n>0} (\hat{\gamma}_{p,0}^\dagger \tilde{F}_{0n}^{i,p} \hat{\gamma}_{p,n} + \hat{\gamma}_{p,n}^\dagger \tilde{F}_{n0}^{i,p} \hat{\gamma}_{p,0}) + \sum_{n,m>0} \hat{\gamma}_{p,n}^\dagger \tilde{F}_{nm}^{i,p} \hat{\gamma}_{p,m} \\ &\approx \tilde{F}_{00}^{i,p} \left(1 - \sum_{n>0} \hat{\gamma}_{p,n}^\dagger \hat{\gamma}_{p,n} \right) + \sum_{n>0} (\tilde{F}_{0n}^{i,p} \hat{\gamma}_{p,n} + \hat{\gamma}_{p,n}^\dagger \tilde{F}_{n0}^{i,p}) + \sum_{n,m>0} \hat{\gamma}_{p,n}^\dagger \tilde{F}_{nm}^{i,p} \hat{\gamma}_{p,m} + O(\hat{\gamma}^3). \end{aligned} \quad (\text{S14})$$

and similarly for the $\hat{b}_{i,p}$ operator. Notice that

$$\psi_{i,p} = \langle \hat{b}_{i,p} \rangle = [\tilde{F}_{00}^{i,p}]^* \quad (\text{S15})$$

It is possible to verify that

$$\begin{aligned} [\tilde{F}_{mn}^{i,p}]^* &= [\tilde{F}_{nm}^{i,p}]^\dagger, \\ [\tilde{F}_{mn}^{i,p}]^* &= \left[\langle \Psi_m^{(p)} | \hat{b}_{i,p}^\dagger | \Psi_n^{(p)} \rangle \right]^* = \left[\langle \hat{b}_{i,p} \Psi_m^{(p)} | \Psi_n^{(p)} \rangle \right]^* = \langle \Psi_n^{(p)} | \hat{b}_{i,p} | \Psi_m^{(p)} \rangle. \end{aligned} \quad (\text{S16})$$

In order to treat bilinears, for example $\hat{b}_{i,p}^\dagger \hat{b}_{j,q}$ for different plaquettes, we expand in terms of \tilde{F} and $\hat{\gamma}$

$$\begin{aligned}
\hat{b}_{i,p}^\dagger \hat{b}_{j,q} &= \left[\sum_{n>0} \tilde{F}_{00}^{i,p} (1 - \hat{\gamma}_{p,n}^\dagger \hat{\gamma}_{p,n}) + \sum_{n>0} (\tilde{F}_{0n}^{i,p} \hat{\gamma}_{p,n} + \hat{\gamma}_{p,n}^\dagger \tilde{F}_{n0}^{i,p}) \sum_{n,m>0} \hat{\gamma}_{p,n}^\dagger \tilde{F}_{nm}^{i,p} \hat{\gamma}_{p,m} \right] \\
&\times \left[\sum_{n'>0} [\tilde{F}_{00}^{j,q}]^* (1 - \hat{\gamma}_{q,n'}^\dagger \hat{\gamma}_{q,n'}) + \sum_{n'>0} ([\tilde{F}_{0n'}^{j,q}]^* \hat{\gamma}_{q,n'}^\dagger + [\tilde{F}_{n'0}^{j,q}]^* \hat{\gamma}_{q,n'}) \sum_{n',m'>0} \hat{\gamma}_{q,m'}^\dagger [\tilde{F}_{n'm'}^{j,q}]^* \hat{\gamma}_{q,n'} \right] = \\
&= \tilde{F}_{00}^{i,p} [\tilde{F}_{00}^{j,q}]^* + \\
&- \tilde{F}_{00}^{i,p} [\tilde{F}_{00}^{j,q}]^* \left(\sum_{n>0} \hat{\gamma}_{p,n}^\dagger \hat{\gamma}_{p,n} + \sum_{n'>0} \hat{\gamma}_{q,n'}^\dagger \hat{\gamma}_{q,n'} \right) + [\tilde{F}_{00}^{j,q}]^* \sum_{n,m>0} \hat{\gamma}_{p,n}^\dagger \tilde{F}_{nm}^{i,p} \hat{\gamma}_{p,m} + \tilde{F}_{00}^{i,p} \sum_{n',m'>0} \hat{\gamma}_{q,m'}^\dagger [\tilde{F}_{n'm'}^{j,q}]^* \hat{\gamma}_{q,n'} + \\
&+ \tilde{F}_{00}^{i,p} \sum_{n'>0} ([\tilde{F}_{0n'}^{j,q}]^* \hat{\gamma}_{q,n'}^\dagger + [\tilde{F}_{n'0}^{j,q}]^* \hat{\gamma}_{q,n'}) + [\tilde{F}_{00}^{j,q}]^* \sum_{n>0} (\tilde{F}_{0n}^{i,p} \hat{\gamma}_{p,n} + \hat{\gamma}_{p,n}^\dagger \tilde{F}_{n0}^{i,p}) + \\
&+ \sum_{n,n'>0} (\tilde{F}_{0n}^{i,p} \hat{\gamma}_{p,n} \hat{\gamma}_{q,n'}^\dagger [\tilde{F}_{0n'}^{j,q}]^* + \hat{\gamma}_{p,n}^\dagger \tilde{F}_{n0}^{i,p} [\tilde{F}_{n'0}^{j,q}]^* \hat{\gamma}_{q,n'}) + \\
&+ \sum_{n,n'>0} (\hat{\gamma}_{p,n}^\dagger \tilde{F}_{n0}^{i,p} \hat{\gamma}_{q,n'}^\dagger [\tilde{F}_{0n'}^{j,q}]^* + \tilde{F}_{0n}^{i,p} \hat{\gamma}_{p,n} [\tilde{F}_{n'0}^{j,q}]^* \hat{\gamma}_{q,n'}) .
\end{aligned} \tag{S17}$$

With this expression we can now work on Eq. (S7) and reduce it to

$$\begin{aligned}
\hat{\mathcal{H}}^{(0)} &= - \sum_{\langle p,q \rangle} \sum_{\langle i,j \rangle} J'_{ij} \tilde{F}_{00}^{i,p} [\tilde{F}_{00}^{j,q}]^* + N \tilde{G}_{00} , \\
\hat{\mathcal{H}}^{(1)} &= \sum_p \sum_{n>0} \hat{\gamma}_{p,n} \langle \Psi_0 | \hat{\mathcal{H}}_{MF}^{(p)} | \Psi_n \rangle + \text{h.c.} , \\
\hat{\mathcal{H}}_{\text{plaq}} &= \sum_p \sum_{n,m>0} \hat{\gamma}_{p,n}^\dagger A_{nm}^{(0)} \hat{\gamma}_{p,m} , \\
\hat{\mathcal{H}}_{\text{hop}} &= \sum_{\langle p,q \rangle} \sum_{n,m>0} \hat{\gamma}_{p,n}^\dagger A_{nm}^{(1)(p,q)} \hat{\gamma}_{q,m} , \\
\hat{\mathcal{H}}_{\text{pairs}} &= \frac{1}{2} \sum_{\langle p,q \rangle} \sum_{n,m>0} \hat{\gamma}_{p,n} B_{nm}^{(p,q)} \hat{\gamma}_{q,m} + \text{h.c.} ,
\end{aligned} \tag{S18}$$

where N is the number of sites. The matrices A and B take the form

$$\begin{aligned}
A_{nm}^{(0)} &= -\delta_{nm} \langle \Psi_0^{(p)} | \mathcal{H}_{MF}^{(p)} | \Psi_0^{(p)} \rangle + \langle \Psi_n^{(p)} | \mathcal{H}_{MF}^{(p)} | \Psi_m^{(p)} \rangle = \delta_{nm} (\epsilon_n - \epsilon_0) ; \\
A_{nm}^{(1)(p,q)} &= - \sum_{\langle i,j \rangle} J'_{ij} (\tilde{F}_{n0}^{i,p} [\tilde{F}_{m0}^{j,q}]^* + \tilde{F}_{0m}^{i,p} [\tilde{F}_{0n}^{j,q}]^*) ; \\
B_{nm}^{(p,q)} &= - \sum_{\langle i,j \rangle} J'_{ij} (\tilde{F}_{0n}^{i,p} [\tilde{F}_{m0}^{j,q}]^* + \tilde{F}_{0m}^{i,p} [\tilde{F}_{n0}^{j,q}]^*) .
\end{aligned} \tag{S19}$$

Since $\hat{\mathcal{H}}_0$ is an offset, while $\hat{\mathcal{H}}_1$ vanishes, the non-vanishing part of the Hamiltonian is

$$\hat{\mathcal{H}}^{(2)} = \hat{\mathcal{H}}_{\text{plaq}} + \hat{\mathcal{H}}_{\text{hop}} + \hat{\mathcal{H}}_{\text{pairs}} . \tag{S20}$$

We focus on our specific case of a cluster of 4 sites in a 2D plaquette configuration, for which we want to find the Fourier transform in order to get the excitation spectrum. We distinguish between vertical hoppings ($U - D$, for example between site (2,p) and (1,p+1)) and horizontal hoppings ($R - L$, for example between site (4,p) and (2,p+1)). The $U - D$ part of $A^{(1)}$ is

$$A_{nm}^{(1)(p,p+1)_{UD}} = \hat{\gamma}_{p,n}^\dagger \underbrace{\left(\tilde{F}_{n0}^{U,p} [\tilde{F}_{m0}^{D,p+1}]^* + [\tilde{F}_{0n}^{U,p}]^* \tilde{F}_{0m}^{D,p+1} \right)}_{A^{(DU)}} \hat{\gamma}_{p+1,m} + \hat{\gamma}_{p+1,n}^\dagger \underbrace{\left([\tilde{F}_{0n}^{D,p+1}]^* \tilde{F}_{0m}^{U,p} + \tilde{F}_{n0}^{D,p+1} [\tilde{F}_{m0}^{U,p}]^* \right)}_{A^{(UD)}} \hat{\gamma}_{p,m} . \tag{S21}$$

With the same procedure we have, for the left-right interaction

$$A_{nm}^{(1)(p,p+1)_{LR}} = \hat{\gamma}_{p,n}^\dagger \underbrace{\left(\tilde{F}_{n0}^{R,p} [\tilde{F}_{m0}^{L,p+1}]^* + [\tilde{F}_{0n}^{R,p}]^* \tilde{F}_{0m}^{L,p+1} \right)}_{A^{(LR)}} \hat{\gamma}_{p+1,m} + \hat{\gamma}_{p+1,n}^\dagger \underbrace{\left([\tilde{F}_{0n}^{L,p+1}]^* \tilde{F}_{0m}^{R,p} + \tilde{F}_{n0}^{L,p+1} [\tilde{F}_{m0}^{R,p}]^* \right)}_{A^{(RL)}} \hat{\gamma}_{p,m} . \quad (\text{S22})$$

We can notice that

$$(A)_{nm} = (A)_{nm}^\dagger , \quad (\text{S23})$$

both for the left-right and up-down interaction, so that we define

$$A_1 = A^{DU} + A^{LR} \quad (\text{S24})$$

$$A_2 = A^{UD} + A^{RL} . \quad (\text{S25})$$

The Fourier transform of γ_p is

$$\hat{\gamma}_p = \frac{1}{\sqrt{N}} \sum_{\mathbf{k}} e^{i\mathbf{k} \cdot \mathbf{r}_p} \hat{\gamma}_{\mathbf{k}} , \quad (\text{S26})$$

with $\mathbf{r}_q = \mathbf{r}_p + \boldsymbol{\delta}$. $\boldsymbol{\delta} = (\hat{\mathbf{u}}_x, \hat{\mathbf{u}}_y)a$ and a is the lattice spacing. If we insert this in (S21)

$$\begin{aligned} A_{\mathbf{k}}^{(1)} &= \frac{1}{N} \sum_p \sum_{\mathbf{k}\mathbf{k}'} \left[e^{-i\mathbf{k} \cdot \mathbf{r}_p} \hat{\gamma}_{\mathbf{k}}^\dagger A_1 e^{i\mathbf{k}' \cdot (\mathbf{r}_p + \boldsymbol{\delta})} \hat{\gamma}_{\mathbf{k}'} + e^{-i\mathbf{k} \cdot (\mathbf{r}_p + \boldsymbol{\delta})} \hat{\gamma}_{\mathbf{k}}^\dagger A_2 e^{i\mathbf{k}' \cdot \mathbf{r}_p} \hat{\gamma}_{\mathbf{k}'} \right] = \\ &= \sum_{\mathbf{k}} \left[e^{i\mathbf{k} \cdot \boldsymbol{\delta}} \hat{\gamma}_{\mathbf{k}}^\dagger A_1 \hat{\gamma}_{\mathbf{k}} + e^{-i\mathbf{k} \cdot \boldsymbol{\delta}} \hat{\gamma}_{\mathbf{k}}^\dagger A_2 \hat{\gamma}_{\mathbf{k}} \right] , \end{aligned}$$

and symmetrizing

$$\begin{aligned} A_{\mathbf{k}}^{(1)} &= \frac{1}{2} \sum_{\mathbf{k}} \left[e^{i\mathbf{k} \cdot \boldsymbol{\delta}} \hat{\gamma}_{\mathbf{k}}^\dagger A_1 \hat{\gamma}_{\mathbf{k}} + e^{-i\mathbf{k} \cdot \boldsymbol{\delta}} \hat{\gamma}_{-\mathbf{k}}^\dagger A_1 \hat{\gamma}_{-\mathbf{k}} + e^{-i\mathbf{k} \cdot \boldsymbol{\delta}} \hat{\gamma}_{\mathbf{k}}^\dagger A_2 \hat{\gamma}_{\mathbf{k}} + e^{i\mathbf{k} \cdot \boldsymbol{\delta}} \hat{\gamma}_{-\mathbf{k}}^\dagger A_2 \hat{\gamma}_{-\mathbf{k}} \right] = \\ &= \frac{1}{2} \sum_{\mathbf{k}} \left[\hat{\gamma}_{\mathbf{k}}^\dagger (e^{i\mathbf{k} \cdot \boldsymbol{\delta}} A_1 + e^{-i\mathbf{k} \cdot \boldsymbol{\delta}} A_2) \hat{\gamma}_{\mathbf{k}} + \underbrace{\hat{\gamma}_{-\mathbf{k}}^\dagger (e^{-i\mathbf{k} \cdot \boldsymbol{\delta}} A_1 + e^{i\mathbf{k} \cdot \boldsymbol{\delta}} A_2) \hat{\gamma}_{-\mathbf{k}}}_{= \hat{\gamma}_{-\mathbf{k}} (e^{-i\mathbf{k} \cdot \boldsymbol{\delta}} A_1 + e^{i\mathbf{k} \cdot \boldsymbol{\delta}} A_2)^T \hat{\gamma}_{-\mathbf{k}}^\dagger} \right] . \end{aligned}$$

We then define $A_{\mathbf{k}} = A^{(0)} + A_{\mathbf{k}}^{(1)}$.

Regarding the B term we have that

$$B_{nm}^{(p,p+1)_{DU}} = \hat{\gamma}_{p,n} \underbrace{\left(\tilde{F}_{0n}^{U,p} [\tilde{F}_{m0}^{D,p+1}]^* + [\tilde{F}_{n0}^{U,p}]^* \tilde{F}_{0m}^{D,p+1} \right)}_{B_1^{DU}} \hat{\gamma}_{p+1,m} + \hat{\gamma}_{p,n}^\dagger \underbrace{\left(\tilde{F}_{n0}^{U,p} [\tilde{F}_{0m}^{D,p+1}]^* + [\tilde{F}_{0n}^{U,p}]^* \tilde{F}_{m0}^{D,p+1} \right)}_{B_2^{DU}} \hat{\gamma}_{p+1,m}^\dagger , \quad (\text{S27})$$

while for the left-right interaction we get

$$B_{nm}^{(p,p+1)_{LR}} = \hat{\gamma}_{p,n} \underbrace{\left(\tilde{F}_{0n}^{R,p} [\tilde{F}_{m0}^{L,p+1}]^* + [\tilde{F}_{n0}^{R,p}]^* \tilde{F}_{0m}^{L,p+1} \right)}_{B_1^{LR}} \hat{\gamma}_{p+1,m} + \hat{\gamma}_{p,n}^\dagger \underbrace{\left(\tilde{F}_{n0}^{R,p} [\tilde{F}_{0m}^{L,p+1}]^* + [\tilde{F}_{0n}^{R,p}]^* \tilde{F}_{m0}^{L,p+1} \right)}_{B_2^{LR}} \hat{\gamma}_{p+1,m}^\dagger . \quad (\text{S28})$$

We notice that

$$(B_1)_{nm} = (B_2)_{nm}^* , \quad (\text{S29})$$

both for the left-right and up-down interaction, so that we define

$$\begin{aligned} B_1 &= B_1^{DU} + B_1^{LR} \\ B_2 &= B_2^{DU} + B_2^{LR} . \end{aligned} \quad (\text{S30})$$

Taking the Fourier transform thanks to (S26) leads to

$$\begin{aligned} B_{\mathbf{k}} &= \sum_{\mathbf{k}, \mathbf{k}'} \left[e^{i\mathbf{k} \cdot \mathbf{r}_p} \hat{\gamma}_{\mathbf{k}} B_1 e^{i\mathbf{k}' \cdot (\mathbf{r}_p + \boldsymbol{\delta})} \hat{\gamma}_{\mathbf{k}'} + e^{-i\mathbf{k} \cdot \mathbf{r}_p} \hat{\gamma}_{\mathbf{k}}^\dagger B_2 e^{i\mathbf{k}' \cdot (\mathbf{r}_p + \boldsymbol{\delta})} \hat{\gamma}_{\mathbf{k}'}^\dagger \right] = \\ &= \sum_{\mathbf{k}} \left[\hat{\gamma}_{\mathbf{k}} B_1 \hat{\gamma}_{-\mathbf{k}} e^{i\mathbf{k} \cdot \boldsymbol{\delta}} + \hat{\gamma}_{\mathbf{k}}^\dagger B_2 \hat{\gamma}_{-\mathbf{k}}^\dagger e^{i\mathbf{k} \cdot \boldsymbol{\delta}} \right] . \end{aligned} \quad (\text{S31})$$

With symmetrization we can get to

$$B_{\mathbf{k}} = \frac{1}{2} \sum_{\mathbf{k}} \left[\hat{\gamma}_{\mathbf{k}} B_1 \hat{\gamma}_{-\mathbf{k}} e^{-i\mathbf{k} \cdot \boldsymbol{\delta}} + \hat{\gamma}_{-\mathbf{k}} B_1 \hat{\gamma}_{\mathbf{k}} e^{i\mathbf{k} \cdot \boldsymbol{\delta}} + \hat{\gamma}_{\mathbf{k}}^\dagger B_2 \hat{\gamma}_{-\mathbf{k}}^\dagger e^{i\mathbf{k} \cdot \boldsymbol{\delta}} + \hat{\gamma}_{-\mathbf{k}}^\dagger B_2 \hat{\gamma}_{\mathbf{k}}^\dagger e^{-i\mathbf{k} \cdot \boldsymbol{\delta}} \right] \quad (\text{S32})$$

$$= \frac{1}{2} \sum_{\mathbf{k}} \left[\hat{\gamma}_{-\mathbf{k}} (B_1^T e^{-i\mathbf{k} \cdot \boldsymbol{\delta}} + B_1 e^{i\mathbf{k} \cdot \boldsymbol{\delta}}) \hat{\gamma}_{\mathbf{k}} + \hat{\gamma}_{\mathbf{k}}^\dagger (B_2 e^{i\mathbf{k} \cdot \boldsymbol{\delta}} + B_2^T e^{-i\mathbf{k} \cdot \boldsymbol{\delta}}) \hat{\gamma}_{-\mathbf{k}}^\dagger \right] \quad (\text{S33})$$

We conclude that the Fourier transform of $\hat{\mathcal{H}}^{(2)}$ can be written as

$$\hat{\mathcal{H}}^{(2)} = \frac{1}{2} \sum_{\mathbf{k}} (\hat{\gamma}_{\mathbf{k}}^\dagger \hat{\gamma}_{-\mathbf{k}}) \underbrace{\begin{pmatrix} A_{\mathbf{k}} & B_{\mathbf{k}} \\ B_{\mathbf{k}}^* & A_{\mathbf{k}}^* \end{pmatrix}}_{\equiv H_{\mathbf{k}}} (\hat{\gamma}_{\mathbf{k}}) + \text{const} . \quad (\text{S34})$$

We now diagonalize the $(2d - 2) \times (2d - 2)$ dimensional matrix

$$\mathcal{M}_{\mathbf{k}} = \begin{pmatrix} \mathbb{1} & 0 \\ 0 & -\mathbb{1} \end{pmatrix} \begin{pmatrix} A_{\mathbf{k}} & B_{\mathbf{k}} \\ B_{\mathbf{k}}^* & A_{\mathbf{k}}^* \end{pmatrix} , \quad (\text{S35})$$

where the minus sign is due to the bosonic character of the particles involved.

To conclude, knowing the eigenspace of the matrix $\mathcal{M}_{\mathbf{k}}$, the quadratic form in (S34) can be diagonalized by applying a suitable Bogoliubov rotation of the slave boson operators

$$\begin{aligned} \hat{\gamma}_{\mathbf{k},n} &= \sum_{\alpha > 0} \left[u_{\alpha, \mathbf{k}, n} \hat{\Gamma}_{\alpha, \mathbf{k}} + v_{\alpha, -\mathbf{k}, n}^* \hat{\Gamma}_{\alpha, -\mathbf{k}}^\dagger \right] \\ \hat{\gamma}_{\mathbf{k},n}^\dagger &= \sum_{\alpha > 0} \left[u_{\alpha, \mathbf{k}, n}^* \hat{\Gamma}_{\alpha, \mathbf{k}}^\dagger + v_{\alpha, -\mathbf{k}, n} \hat{\Gamma}_{\alpha, -\mathbf{k}} \right] , \end{aligned} \quad (\text{S36})$$

where n runs among the levels of excitation. The diagonalized Hamiltonian then takes the form

$$\hat{\mathcal{H}}^{(2)} = \sum_{\mathbf{k}} \sum_{\alpha > 0} \hbar \omega_{\alpha, \mathbf{k}} \hat{\Gamma}_{\alpha, \mathbf{k}}^\dagger \hat{\Gamma}_{\alpha, \mathbf{k}} , \quad (\text{S37})$$

from which we get the plot in Fig. S2.

OBSERVABLES

Here we show in detail the expressions for the flatness, the density and the loop current shown in the main text. We start from the flatness, which is the first order correction to the order parameter. From (S14) and thanks to (S36) it is possible to write the destruction operator as

$$\begin{aligned} \hat{b}_{i,p} &= [\tilde{F}_{00}^{i,p}]^* + \\ &- [\tilde{F}_{00}^{i,p}]^* \sum_{n > 0} \frac{1}{N} \sum_{\mathbf{k}, \mathbf{k}'} e^{-i(\mathbf{k} - \mathbf{k}') \cdot \mathbf{r}_p} \sum_{\alpha, \beta > 0} \left(u_{\alpha, \mathbf{k}, n}^* \hat{\Gamma}_{\alpha, \mathbf{k}}^\dagger + v_{\alpha, -\mathbf{k}, n} \hat{\Gamma}_{\alpha, -\mathbf{k}} \right) \left(u_{\alpha, \mathbf{k}, n}^* \hat{\Gamma}_{\alpha, \mathbf{k}}^\dagger + v_{\alpha, -\mathbf{k}, n} \hat{\Gamma}_{\alpha, -\mathbf{k}} \right) + \\ &+ \sum_{n > 0} \frac{1}{\sqrt{N}} [\tilde{F}_{0n}^{i,p}]^* \sum_{\mathbf{k}} e^{-i\mathbf{k} \cdot \mathbf{r}_p} \sum_{\alpha > 0} \left(u_{\alpha, \mathbf{k}, n}^* \hat{\Gamma}_{\alpha, \mathbf{k}}^\dagger + v_{\alpha, -\mathbf{k}, n} \hat{\Gamma}_{\alpha, -\mathbf{k}} \right) + \\ &+ \sum_{n > 0} \frac{1}{\sqrt{N}} [\tilde{F}_{n0}^{i,p}]^* \sum_{\mathbf{k}} e^{i\mathbf{k} \cdot \mathbf{r}_p} \sum_{\alpha > 0} \left(u_{\alpha, \mathbf{k}, n} \hat{\Gamma}_{\alpha, \mathbf{k}} + v_{\alpha, -\mathbf{k}, n}^* \hat{\Gamma}_{\alpha, -\mathbf{k}}^\dagger \right) + \\ &+ \sum_{n, m > 0} [\tilde{F}_{nm}^{i,p}]^* \frac{1}{N} \sum_{\mathbf{k}, \mathbf{k}'} e^{-i(\mathbf{k} - \mathbf{k}') \cdot \mathbf{r}_p} \sum_{\alpha, \beta > 0} \left(u_{\alpha, \mathbf{k}, m}^* \hat{\Gamma}_{\alpha, \mathbf{k}}^\dagger + v_{\alpha, -\mathbf{k}, m} \hat{\Gamma}_{\alpha, -\mathbf{k}} \right) \left(u_{\alpha, \mathbf{k}, m}^* \hat{\Gamma}_{\alpha, \mathbf{k}}^\dagger + v_{\alpha, -\mathbf{k}, m} \hat{\Gamma}_{\alpha, -\mathbf{k}} \right) . \end{aligned} \quad (\text{S38})$$

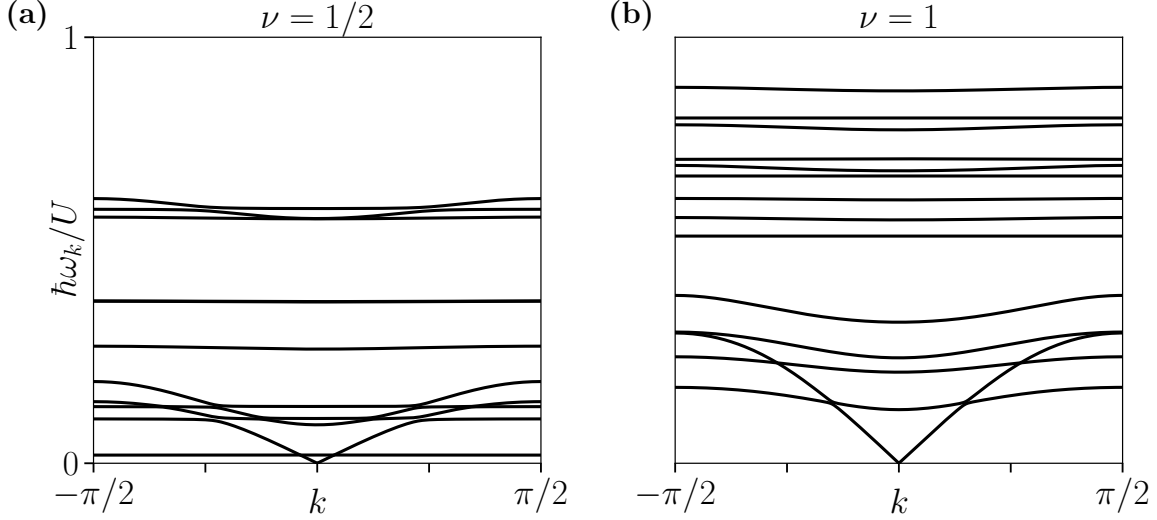


Figure S2. First excitations bands computed with the slave boson approach for (a) $\nu = 1/2$ at $J'/U = 0.02$, $J/U = 0.67$, and $\mu/U = 0.67$, with $|\mathbf{k}_x| = |\mathbf{k}_y| = k$ and for (b) $\nu = 1$ at $J'/U = 0.03$, $J/U = 1$, and $\mu/U = -0.68$, with $|\mathbf{k}_x| = |\mathbf{k}_y| = k$.

Within linear-response theory, we consider a generic excited state as composed of the ground state $|\tilde{g}\rangle$ component and an excitation $|\tilde{e}\rangle$ component,

$$|\tilde{\Psi}_\alpha\rangle = |\tilde{g}\rangle + \varepsilon|\tilde{e}_\alpha\rangle, \quad (\text{S39})$$

where $\hat{\Gamma}_\alpha|\tilde{g}\rangle = 0$ and $\varepsilon \ll 1$. The expectation value of the destruction operator reads

$$\langle \tilde{\Psi}_\alpha | \hat{b}_{i,p} | \tilde{\Psi}_\alpha \rangle = \langle \tilde{g} | \hat{b}_{i,p} | \tilde{g} \rangle + \varepsilon (\langle \tilde{g} | \hat{b}_{i,p} | \tilde{e}_\alpha \rangle + \langle \tilde{e}_\alpha | \hat{b}_{i,p} | \tilde{g} \rangle) = \psi^{i,p} + \varepsilon \delta_1 \psi^{i,p} + o(\varepsilon^2), \quad (\text{S40})$$

where the first term is the ground state superfluid order parameter and the second term its fluctuation due to the excitation $|\tilde{e}_\alpha\rangle$. At first order in ε the only non zero terms are

$$\delta_1 \hat{\psi}^{i,p} = \frac{1}{\sqrt{N}} \sum_{\alpha>0} \sum_{\mathbf{k}} \sum_{n>0} \left[e^{i\mathbf{k}\cdot\mathbf{r}_p} \left([\tilde{F}_{n0}^{i,p}]^* u_{\alpha,\mathbf{k},n} + [\tilde{F}_{0n}^{i,p}]^* v_{\alpha,\mathbf{k},n} \right) \hat{\Gamma}_{\alpha,\mathbf{k}} + e^{-i\mathbf{k}\cdot\mathbf{r}_p} \left([\tilde{F}_{0n}^{i,p}]^* u_{\alpha,\mathbf{k},n}^* + [\tilde{F}_{n0}^{i,p}]^* v_{\alpha,\mathbf{k},n}^* \right) \hat{\Gamma}_{\alpha,\mathbf{k}}^\dagger \right], \quad (\text{S41})$$

where we can recognize

$$\mathcal{U}_{\alpha,\mathbf{k}} = \sum_{n>0} \left[[\tilde{F}_{n0}^{i,p}]^* u_{\alpha,\mathbf{k},n} + [\tilde{F}_{0n}^{i,p}]^* v_{\alpha,\mathbf{k},n} \right] \quad (\text{S42})$$

$$\mathcal{V}_{\alpha,\mathbf{k}} = \sum_{n>0} \left[[\tilde{F}_{0n}^{i,p}]^* u_{\alpha,\mathbf{k},n}^* + [\tilde{F}_{n0}^{i,p}]^* v_{\alpha,\mathbf{k},n}^* \right]. \quad (\text{S43})$$

that correspond to those used in [80, 81]. We can then define the real and imaginary part of $\delta_1 \psi^{i,p}$ as $\mathcal{R}_{\alpha,\mathbf{k}} = |\mathcal{U}_{\alpha,\mathbf{k}} + \mathcal{V}_{\alpha,\mathbf{k}}|$ and $\mathcal{I}_{\alpha,\mathbf{k}} = |\mathcal{U}_{\alpha,\mathbf{k}} - \mathcal{V}_{\alpha,\mathbf{k}}|$. We are in presence of a pure amplitude mode when $\mathcal{I}_{\alpha,\mathbf{k}} = 0$, while pure phase excitations of the order parameter corresponds to $\mathcal{R}_{\alpha,\mathbf{k}} = 0$.

In this way, the flatness parameter studies the evolution between pure amplitude and phase modes and it is defined as

$$\mathcal{F}_{\alpha,\mathbf{k}} = \frac{\mathcal{R}_{\alpha,\mathbf{k}} - \mathcal{I}_{\alpha,\mathbf{k}}}{\mathcal{R}_{\alpha,\mathbf{k}} + \mathcal{I}_{\alpha,\mathbf{k}}} \in [-1, 1]. \quad (\text{S44})$$

Another relevant observable is the density $\hat{n}_i = \langle b_i^\dagger b_j \rangle$ for each site i . Since this time we are treating \hat{b} operators in the same plaquette (cluster) p we can not consider the expression used in (S17), where we had to consider \hat{b} and \hat{b}^\dagger

as totally uncorrelated operators. We derive then $\hat{b}_{i,p}^\dagger \hat{b}_{i,p}$ in the following way

$$\begin{aligned}
\hat{b}_{i,p}^\dagger \hat{b}_{i,p} &= \sum_{n,m} \left(\hat{\gamma}_{n,p}^\dagger \tilde{F}_{nm}^{i,p} \hat{\gamma}_{m,p} \right) \times \sum_{n',m'} \left(\hat{\gamma}_{n',p}^\dagger [\tilde{F}_{m'n'}^{i,p}]^* \hat{\gamma}_{m',p} \right) = \\
&= \sum_{n,m} \left[\sum_{\mathbf{n}} \left(\langle \mathbf{n} | \Psi_n^{(p)} \rangle \beta_{p,\mathbf{n}}^\dagger \right) \langle \Psi_n^{(p)} | \hat{b}_{i,p}^\dagger | \Psi_m^{(p)} \rangle \sum_{\mathbf{m}} \left(\langle \Psi_m^{(p)} | \mathbf{m} \rangle \beta_{p,\mathbf{m}} \right) \right] \times \\
&\quad \times \sum_{n',m'} \left[\sum_{\mathbf{n}'} \left(\langle \mathbf{n}' | \Psi_{n'}^{(p)} \rangle \beta_{p,\mathbf{n}'}^\dagger \right) \langle \Psi_{n'}^{(p)} | \hat{b}_{i,p}^\dagger | \Psi_{m'}^{(p)} \rangle \sum_{\mathbf{m}'} \left(\langle \Psi_{m'}^{(p)} | \mathbf{m}' \rangle \beta_{p,\mathbf{m}'} \right) \right] = \\
&= \sum_{\substack{\mathbf{n}, \mathbf{n}' \\ \mathbf{m}, \mathbf{m}'}} \langle \mathbf{n} | b_{i,p}^\dagger | \mathbf{m} \rangle \langle \mathbf{n}' | b_{i,p} | \mathbf{m}' \rangle \beta_{p,\mathbf{n}}^\dagger \beta_{p,\mathbf{m}} \beta_{p,\mathbf{n}'}^\dagger \beta_{p,\mathbf{m}'} = \\
&= \sum_{\substack{\mathbf{n}, \mathbf{n}' \\ \mathbf{m}, \mathbf{m}'}} \langle \mathbf{n} | b_{i,p}^\dagger | \mathbf{m} \rangle \langle \mathbf{n}' | b_{i,p} | \mathbf{m}' \rangle \beta_{p,\mathbf{n}}^\dagger \beta_{p,\mathbf{m}'} \delta_{\mathbf{m}, \mathbf{n}'} + \sum_{\substack{\mathbf{n}, \mathbf{n}' \\ \mathbf{m}, \mathbf{m}'}} \langle \mathbf{n} | b_{i,p}^\dagger | \mathbf{m} \rangle \langle \mathbf{n}' | b_{i,p} | \mathbf{m}' \rangle \beta_{p,\mathbf{n}}^\dagger \beta_{p,\mathbf{n}'}^\dagger \beta_{p,\mathbf{m}'} \beta_{p,\mathbf{m}'} = \\
&= \sum_{\substack{\mathbf{n} \\ \mathbf{m}, \mathbf{m}'}} \langle \mathbf{n} | b_{i,p}^\dagger | \mathbf{m} \rangle \langle \mathbf{m} | b_{i,p} | \mathbf{m}' \rangle \beta_{p,\mathbf{n}}^\dagger \beta_{p,\mathbf{m}'} = \\
&= \sum_{\mathbf{n}, \mathbf{m}'} \langle \mathbf{n} | b_{i,p}^\dagger b_{i,p} | \mathbf{m}' \rangle \beta_{p,\mathbf{n}}^\dagger \beta_{p,\mathbf{m}'}.
\end{aligned} \tag{S45}$$

The canceled contribution would take nonzero values only when annihilating two occupied states \mathbf{m} , \mathbf{m}' via the operators $\beta_{p,\mathbf{m}} \beta_{p,\mathbf{m}'}$, but two occupied SB states are not possible because of the slave boson constraint

$$\sum_{\mathbf{n}} \beta_{p,\mathbf{n}}^\dagger \beta_{p,\mathbf{n}} = 1, \tag{S46}$$

and we are thus left with the first term only. Going back to the $\hat{\gamma}$ operators notation we have

$$\begin{aligned}
\hat{b}_{i,p}^\dagger \hat{b}_{i,p} &= \sum_{\mathbf{n}, \mathbf{m}'} \sum_n \langle \Psi_n | \mathbf{n} \rangle \hat{\gamma}_{p,n}^\dagger \langle \mathbf{n} | b_{i,p}^\dagger b_{i,p} | \mathbf{m}' \rangle \sum_m \langle \mathbf{m}' | \Psi_m \rangle \hat{\gamma}_{p,m} = \\
&= \sum_{n,m} \langle \Psi_n | b_{i,p}^\dagger b_{i,p} | \Psi_m \rangle \hat{\gamma}_{p,n}^\dagger \hat{\gamma}_{p,m}.
\end{aligned} \tag{S47}$$

In order to perform the condensation on the $\hat{\gamma}_0$ operators we expand

$$\begin{aligned}
\hat{n}_{i,p} &= \langle \Psi_0 | \hat{b}_{i,p}^\dagger \hat{b}_{i,p} | \Psi_0 \rangle \underbrace{\hat{\gamma}_{p,0}^\dagger \hat{\gamma}_{p,0}}_{1 - \sum_{n>0} \hat{\gamma}_{p,n}^\dagger \hat{\gamma}_{p,n}} + \\
&\quad + \sum_{n>0} \left[\hat{\gamma}_{p,n}^\dagger \langle \Psi_n | \hat{b}_{i,p}^\dagger \hat{b}_{i,p} | \Psi_0 \rangle \hat{\gamma}_0 + \hat{\gamma}_{p,0}^\dagger \langle \Psi_0 | \hat{b}_{i,p}^\dagger \hat{b}_{i,p} | \Psi_n \rangle \hat{\gamma}_{p,n} \right] + \\
&\quad + \sum_{n,m>0} \hat{\gamma}_{p,n}^\dagger \langle \Psi_n | \hat{b}_{i,p}^\dagger \hat{b}_{i,p} | \Psi_m \rangle \hat{\gamma}_{p,m} = \\
&= \langle \Psi_0 | \hat{b}_{i,p}^\dagger \hat{b}_{i,p} | \Psi_0 \rangle \left(1 - \sum_{n>0} \hat{\gamma}_{p,n}^\dagger \hat{\gamma}_{p,n} \right) + \sum_{n>0} \left[\hat{\gamma}_{p,n}^\dagger \langle \Psi_n | \hat{b}_{i,p}^\dagger \hat{b}_{i,p} | \Psi_0 \rangle + \langle \Psi_0 | \hat{b}_{i,p}^\dagger \hat{b}_{i,p} | \Psi_n \rangle \hat{\gamma}_{p,n} \right] + \\
&\quad + \sum_{n,m>0} \hat{\gamma}_{p,n}^\dagger \langle \Psi_n | \hat{b}_{i,p}^\dagger \hat{b}_{i,p} | \Psi_m \rangle \hat{\gamma}_{p,m}.
\end{aligned} \tag{S48}$$

The first term in (S48) corresponds to the mean-field contribution of the ground state

$$\delta_0 \hat{n}_{i,p} = \langle \Psi_0 | \hat{b}_{i,p}^\dagger \hat{b}_{i,p} | \Psi_0 \rangle = \sum_n |\tilde{F}_{0n}^{i,p}|^2. \tag{S49}$$

The second term is instead the first order correction to the density

$$\delta_1 \hat{n}_{i,p} = \sum_{n>0,m} \left(\tilde{F}_{nm}^{i,p} [\tilde{F}_{0m}^{i,p}]^* \hat{\gamma}_{p,n}^\dagger + \tilde{F}_{0m}^{i,p} [\tilde{F}_{nm}^{i,p}]^* \hat{\gamma}_{p,n} \right), \quad (\text{S50})$$

and if we apply the Fourier transform defined before we get

$$\begin{aligned} \delta_1 \hat{n}_{i,p} &= \frac{1}{\sqrt{N}} \sum_{\alpha>0} \sum_{\mathbf{k}} \sum_{n>0,m} \left(\tilde{F}_{nm}^{i,p} [\tilde{F}_{0m}^{i,p}]^* v_{\alpha,\mathbf{k},n} + \tilde{F}_{0m}^{i,p} [\tilde{F}_{nm}^{i,p}]^* u_{\alpha,\mathbf{k},n} \right) e^{i\mathbf{k}\cdot\mathbf{r}_p} \hat{\Gamma}_{\alpha,\mathbf{k}} + \\ &+ \frac{1}{\sqrt{N}} \sum_{\alpha>0} \sum_{\mathbf{k}} \sum_{n>0,m} \left(\tilde{F}_{nm}^{i,p} [\tilde{F}_{0m}^{i,p}]^* u_{\alpha,\mathbf{k},n}^* + \tilde{F}_{0m}^{i,p} [\tilde{F}_{nm}^{i,p}]^* v_{\alpha,\mathbf{k},n}^* \right) e^{-i\mathbf{k}\cdot\mathbf{r}_p} \hat{\Gamma}_{\alpha,\mathbf{k}}^\dagger. \end{aligned} \quad (\text{S51})$$

The second order correction to the density operator is the one quadratic in $\hat{\gamma}_{p,n}$ operators and can be computed from (S48)

$$\begin{aligned} \delta_2 \hat{n}_{i,p} &= - \sum_n \langle \Psi_0 | b_{i,p}^\dagger | \Psi_n \rangle \langle \Psi_n | b_{i,p} | \Psi_0 \rangle \sum_{m>0} \hat{\gamma}_{p,m}^\dagger \hat{\gamma}_{p,m} + \sum_{n,m>0} \sum_l \hat{\gamma}_{p,n}^\dagger \langle \Psi_n | b_{i,p}^\dagger | \Psi_l \rangle \langle \Psi_l | b_{i,p} | \Psi_m \rangle \hat{\gamma}_{p,m} = \\ &= - \sum_n |\tilde{F}_{0n}^{i,p}|^2 \sum_{m>0} \hat{\gamma}_{p,m}^\dagger \hat{\gamma}_{p,m} + \sum_{n,m>0,l} \tilde{F}_{nl}^{i,p} [\tilde{F}_{ml}^{i,p}]^* \hat{\gamma}_{p,n}^\dagger \hat{\gamma}_{p,m} = \\ &= - \sum_l |\tilde{F}_{0l}^{i,p}|^2 \sum_{m>0} \frac{1}{N} \sum_{\alpha>0} \sum_{\mathbf{k},\mathbf{k}'} e^{-i(\mathbf{k}-\mathbf{k}')\cdot\mathbf{r}_p} \hat{\gamma}_{\mathbf{k},m}^\dagger \hat{\gamma}_{\mathbf{k}',m} + \\ &+ \sum_{n,m>0,l} \tilde{F}_{nl}^{i,p} [\tilde{F}_{ml}^{i,p}]^* \frac{1}{N} \sum_{\alpha>0} \sum_{\mathbf{k},\mathbf{k}'} e^{-i(\mathbf{k}-\mathbf{k}')\cdot\mathbf{r}_p} \hat{\gamma}_{\mathbf{k},n}^\dagger \hat{\gamma}_{\mathbf{k}',m}. \end{aligned} \quad (\text{S52})$$

From this expression we apply the usual Bogoliubov transformation (S36) to get

$$\begin{aligned} \delta_2 \hat{n}_{i,p} &= - \sum_l |\tilde{F}_{0l}^{i,p}|^2 \cdot \sum_{m>0} \frac{1}{N} \sum_{\mathbf{k},\mathbf{k}'} e^{-i(\mathbf{k}-\mathbf{k}')\cdot\mathbf{r}_p} \sum_{\alpha,\beta>0} \left(u_{\alpha,\mathbf{k},m}^* \hat{\Gamma}_{\alpha,\mathbf{k}}^\dagger + v_{\alpha,-\mathbf{k},m} \hat{\Gamma}_{\alpha,-\mathbf{k}} \right) \left(u_{\beta,\mathbf{k}',m} \hat{\Gamma}_{\beta,\mathbf{k}'} + v_{\alpha,-\mathbf{k}',m}^* \hat{\Gamma}_{\beta,-\mathbf{k}'}^\dagger \right) + \\ &+ \sum_{n,m>0,l} \tilde{F}_{nl}^{i,p} [\tilde{F}_{ml}^{i,p}]^* \frac{1}{N} \sum_{\mathbf{k},\mathbf{k}'} e^{-i(\mathbf{k}-\mathbf{k}')\cdot\mathbf{r}_p} \sum_{\alpha,\beta>0} \left(u_{\alpha,\mathbf{k},n}^* \hat{\Gamma}_{\alpha,\mathbf{k}}^\dagger + v_{\alpha,-\mathbf{k},n} \hat{\Gamma}_{\alpha,-\mathbf{k}} \right) \left(u_{\beta,\mathbf{k}',n} \hat{\Gamma}_{\beta,\mathbf{k}'} + v_{\alpha,-\mathbf{k}',n}^* \hat{\Gamma}_{\beta,-\mathbf{k}'}^\dagger \right). \end{aligned} \quad (\text{S53})$$

With (S52) we can also compute the expectation value of the density on the excited states. Indicating $|\bar{\alpha}, \bar{\mathbf{k}}\rangle \equiv \hat{\gamma}_{\bar{\alpha}, \bar{\mathbf{k}}}^\dagger |\bar{g}\rangle$ as the excited state, the density expectation value reads

$$\langle \hat{n}_{i,p} \rangle_{\bar{\alpha}, \bar{\mathbf{k}}} = \langle \delta_0 \hat{n}_{i,p} \rangle + \langle \delta_2 \hat{n}_{i,p} \rangle_{\bar{\alpha}, \bar{\mathbf{k}}}. \quad (\text{S54})$$

Here $n_{i,p}^0$ is the mean-field density of the ground state for the site i of the p -th plaquette. In particular we get

$$\begin{aligned} \langle \delta_2 \hat{n}_{i,p} \rangle_{\bar{\alpha}, \bar{\mathbf{k}}} &= - \frac{1}{N} \sum_l \left[|\tilde{F}_{0l}^{i,p}|^2 \sum_{m>0} \left(|u_{\bar{\alpha}, \bar{\mathbf{k}}, m}|^2 + |v_{\bar{\alpha}, \bar{\mathbf{k}}, m}|^2 + \sum_{\mathbf{k}} \sum_{\alpha>0} |v_{\alpha, \mathbf{k}, m}|^2 \right) \right] + \\ &+ \frac{1}{N} \sum_{n,m>0,l} \left[\tilde{F}_{nl}^{i,p} [\tilde{F}_{ml}^{i,p}]^* \left(u_{\bar{\alpha}, \bar{\mathbf{k}}, n}^* u_{\bar{\alpha}, \bar{\mathbf{k}}, m} + v_{\bar{\alpha}, \bar{\mathbf{k}}, n}^* v_{\bar{\alpha}, \bar{\mathbf{k}}, m} + \sum_{\alpha>0} \sum_{\mathbf{k}} v_{\alpha, \mathbf{k}, n}^* v_{\alpha, \mathbf{k}, m} \right) \right] = \\ &= - \frac{1}{N} \sum_l \left[|\tilde{F}_{0l}^{i,p}|^2 \sum_{m>0} \left(|u_{\bar{\alpha}, \bar{\mathbf{k}}, m}|^2 + |v_{\bar{\alpha}, \bar{\mathbf{k}}, m}|^2 \right) \right] + \frac{1}{N} \sum_{n,m>0,l} \left[\tilde{F}_{nl}^{i,p} [\tilde{F}_{ml}^{i,p}]^* \left(u_{\bar{\alpha}, \bar{\mathbf{k}}, n}^* u_{\bar{\alpha}, \bar{\mathbf{k}}, m} + v_{\bar{\alpha}, \bar{\mathbf{k}}, n}^* v_{\bar{\alpha}, \bar{\mathbf{k}}, m} \right) \right] + \\ &+ \sum_{\mathbf{k}} (\dots). \end{aligned} \quad (\text{S55})$$

From this expression, we derive the results for the density variations of the different modes displayed in the main text in the saddle point approximation, namely we did not include the quantum fluctuations (i.e., the $\sum_{\mathbf{k}}$ terms in

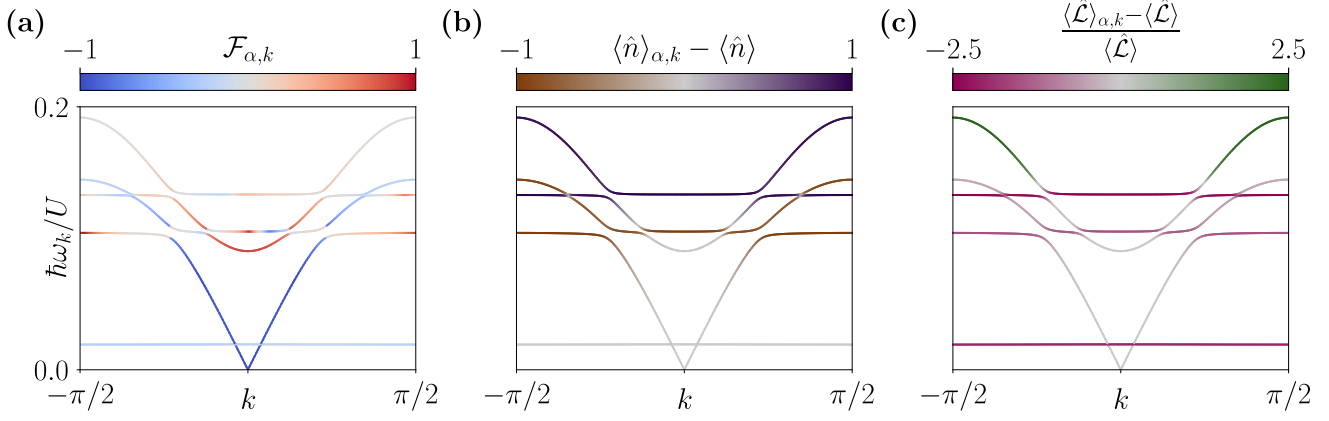


Figure S3. Low-energy excitation spectrum for filling $\nu = 1/2$ at $J'/U = 0.02$, $J/U = 0.67$, and $\mu/U = -0.67$, with $|\mathbf{k}_x| = |\mathbf{k}_y| = k$. **(a)** Flatness $\mathcal{F}_{\alpha,k}$ of the excitation bands, showing the gapless Goldstone mode (blue) and an amplitude (Higgs) mode (red). The flat bands present different values of flatness due to band crossings. **(b)** Plaquette density, showing two bands with particle and hole excitations. **(c)** Loop current $\langle \hat{L}_{\alpha,k} \rangle$ for each band relative to the ground-state current $\langle \hat{L} \rangle$. The Higgs mode carries a loop current with the same sign as the ground state one.

the previous expression). Notice that for the Goldstone mode ($\bar{\alpha} = 1$), a divergence occurs when including for $\bar{\mathbf{k}} = 0$ since the Bogoliubov coefficients $v_{1,\mathbf{k},n}$ diverge at $\mathbf{k} \rightarrow 0$, as in standard bosonic gases.

The last observable we want to compute is the loop current. We focus on the correlator $\langle \hat{b}_{i,p}^\dagger \hat{b}_{j,p} \rangle$: the loop current will be a linear combination of some of this term for each plaquette, as shown in the main text. We can write

$$\langle \hat{b}_{i,p}^\dagger \hat{b}_{j,p} \rangle_{\bar{\alpha}, \bar{\mathbf{k}}} = \langle \delta_0(\hat{b}_{i,p}^\dagger \hat{b}_{j,p}) \rangle + \langle \delta_1(\hat{b}_{i,p}^\dagger \hat{b}_{j,p}) \rangle + \langle \delta_2(\hat{b}_{i,p}^\dagger \hat{b}_{j,p}) \rangle, \quad (\text{S56})$$

The ground state value is

$$\langle \delta_0(\hat{b}_{i,p}^\dagger \hat{b}_{j,p}) \rangle = \sum_n \tilde{F}_{0n}^{i,p} [\tilde{F}_{0n}^{j,p}]^*. \quad (\text{S57})$$

Recalling (S51) it is possible to show the first order correction to this two site correlator, which takes the form

$$\begin{aligned} \delta_1(\hat{b}_{i,p}^\dagger \hat{b}_{j,p}) &= \frac{1}{\sqrt{N}} \sum_{\mathbf{k}} \sum_{n>0, m} \sum_{\alpha>0} \left(\tilde{F}_{nm}^{i,p} [\tilde{F}_{0m}^{j,p}]^* v_{\alpha,\mathbf{k},n} + \tilde{F}_{0m}^{i,p} [\tilde{F}_{nm}^{j,p}]^* v_{\alpha,\mathbf{k},n} \right) e^{i\mathbf{k} \cdot \mathbf{r}_p} \hat{\Gamma}_{\alpha,\mathbf{k}} + \\ &+ \frac{1}{\sqrt{N}} \sum_{\mathbf{k}} \sum_{n>0, m} \sum_{\alpha>0} \left(\tilde{F}_{nm}^{i,p} [\tilde{F}_{0m}^{j,p}]^* u_{\alpha,\mathbf{k},n}^* + \tilde{F}_{0m}^{i,p} [\tilde{F}_{nm}^{j,p}]^* v_{\alpha,\mathbf{k},n}^* \right) e^{-i\mathbf{k} \cdot \mathbf{r}_p} \hat{\Gamma}_{\alpha,\mathbf{k}}^\dagger. \end{aligned} \quad (\text{S58})$$

The second order correction can be instead written as

$$\begin{aligned} \delta_2(\hat{b}_{i,p}^\dagger \hat{b}_{j,p}) &= - \sum_l \tilde{F}_{0l}^{i,p} [\tilde{F}_{0l}^{j,p}]^* \cdot \sum_{m>0} \frac{1}{N} \sum_{\mathbf{k}, \mathbf{k}'} e^{-i(\mathbf{k}-\mathbf{k}') \cdot \mathbf{r}_p} \sum_{\alpha, \beta>0} \left(u_{\alpha,\mathbf{k},m}^* \hat{\Gamma}_{\alpha,\mathbf{k}}^\dagger + v_{\alpha,-\mathbf{k},m} \hat{\Gamma}_{\alpha,-\mathbf{k}} \right) \left(u_{\beta,\mathbf{k}',m} \hat{\Gamma}_{\beta,\mathbf{k}'} + v_{\alpha,-\mathbf{k}',m}^* \hat{\Gamma}_{\beta,-\mathbf{k}'}^\dagger \right) + \\ &+ \sum_{n, m>0, l} \tilde{F}_{nl}^{i,p} [\tilde{F}_{ml}^{j,p}]^* \frac{1}{N} \sum_{\mathbf{k}, \mathbf{k}'} e^{-i(\mathbf{k}-\mathbf{k}') \cdot \mathbf{r}_p} \sum_{\alpha, \beta>0} \left(u_{\alpha,\mathbf{k},n}^* \hat{\Gamma}_{\alpha,\mathbf{k}}^\dagger + v_{\alpha,-\mathbf{k},n} \hat{\Gamma}_{\alpha,-\mathbf{k}} \right) \left(u_{\beta,\mathbf{k}',m} \hat{\Gamma}_{\beta,\mathbf{k}'} + v_{\alpha,-\mathbf{k}',m}^* \hat{\Gamma}_{\beta,-\mathbf{k}'}^\dagger \right). \end{aligned} \quad (\text{S59})$$

In order to compute the loop current for the bands in the excitation spectra, since $\langle \delta_1(\hat{b}_{i,p}^\dagger \hat{b}_{j,p}) \rangle = 0$ we can write

$$\langle \hat{b}_{i,p}^\dagger \hat{b}_{j,p} \rangle_{\bar{\alpha}, \bar{\mathbf{k}}} = \langle \delta_0(\hat{b}_{i,p}^\dagger \hat{b}_{j,p}) \rangle + \langle \delta_2(\hat{b}_{i,p}^\dagger \hat{b}_{j,p}) \rangle_{\bar{\alpha}, \bar{\mathbf{k}}} \quad (\text{S60})$$

If we focus on the last term we can get

$$\begin{aligned}
\langle \delta_2(\hat{b}_{i,p}^\dagger \hat{b}_{j,p}) \rangle_{\bar{\alpha}, \bar{\mathbf{k}}} &= - \sum_n \tilde{F}_{n0}^{i,p} [\tilde{F}_{n0}^{j,p}]^* \sum_{m>0} \left(|u_{\bar{\alpha}, \bar{\mathbf{k}}, m}|^2 + |v_{\bar{\alpha}, \bar{\mathbf{k}}, m}|^2 + \frac{1}{N} \sum_{\mathbf{k}} \sum_{\alpha>0} |v_{\alpha, \mathbf{k}, m}|^2 \right) + \\
&+ \sum_{n,m>0} \sum_l \left[\tilde{F}_{nl}^{i,p} [\tilde{F}_{ml}^{j,p}]^* \left(u_{\bar{\alpha}, \bar{\mathbf{k}}, n}^* u_{\bar{\alpha}, \bar{\mathbf{k}}, m} + v_{\bar{\alpha}, \bar{\mathbf{k}}, n} v_{\bar{\alpha}, \bar{\mathbf{k}}, m}^* + \frac{1}{N} \sum_{\mathbf{k}} \sum_{\alpha>0} v_{\alpha, \mathbf{k}, n} v_{\alpha, \mathbf{k}, m}^* \right) \right] = \\
&= - \sum_n \tilde{F}_{n0}^{i,p} [\tilde{F}_{n0}^{j,p}]^* \sum_{m>0} \left(|u_{\bar{\alpha}, \bar{\mathbf{k}}, m}|^2 + |v_{\bar{\alpha}, \bar{\mathbf{k}}, m}|^2 \right) + \sum_{n,m>0} \sum_l \left[\tilde{F}_{nl}^{i,p} [\tilde{F}_{ml}^{j,p}]^* \left(u_{\bar{\alpha}, \bar{\mathbf{k}}, n}^* u_{\bar{\alpha}, \bar{\mathbf{k}}, m} + v_{\bar{\alpha}, \bar{\mathbf{k}}, n} v_{\bar{\alpha}, \bar{\mathbf{k}}, m}^* \right) \right] \\
&+ \sum_{\mathbf{k}} (\dots) ,
\end{aligned} \tag{S61}$$

which is the expression we used to compute the loop current for the lowest excitation bands. As for the density, we neglect the quantum fluctuations and the $\bar{\mathbf{k}} = \mathbf{0}$ point for $\bar{\alpha} = 1$ (Goldstone). In the main text, we focused on the transition between the trivial Mott insulating and vortex superfluid phases at integer filling. Here, we extend the analysis to fractional fillings using the Gutzwiller mean-field approach. For the three cases of interest, $\nu = 3/4, 1/2$, and $1/4$, we find the same qualitative behavior: a transition between a vortex insulating and a vortex superfluid phase. As shown in Fig. S3, which reports the excitation spectrum for $\nu = 1/2$, the low-energy physics is governed by five excitation bands. Panel (a) reveals the presence of a gapless Goldstone mode and a single Higgs (amplitude) mode. In addition, we identify particle and hole branches, together with a fifth flat band characterized by nearly constant density and a flatness $\mathcal{F}_{k \sim \pi/100} \approx 0$. From panel (c), we infer that this flat band carries an angular momentum opposite to that of the ground state. In contrast, the Higgs mode exhibits the same angular momentum as the ground state $\langle \hat{L} \rangle$. This amplitude mode hybridizes with the Goldstone mode at the transition point, giving rise to a Vortex-Mott Insulating phase. In this case, only the U(1) symmetry is broken, since the discrete \mathbb{Z}_2 symmetry is broken also in the vortex-superfluid phase. In such time-reversal broken phase, the low-energy behaviour described by the quasiparticles is not different from the one in the conventional Bose-Hubbard model. As we have seen, a different scenario instead takes place at integer filling.

B. ADDITIONAL DMRG RESULTS AND DETAILS.

To further support the cluster Gutzwiller results, we perform density-matrix renormalization group (DMRG) simulations of the bosonic BBH model on a ladder geometry. We analyze several observables to characterize the phase transitions at fillings $\nu = 1$ and $\nu = 1/4$. A central quantity is the fidelity susceptibility,

$$\chi_{\mathcal{F}} = - \frac{1}{L} \frac{\langle \psi(U + \delta U) | \psi(U) \rangle \langle \psi(U - \delta U) | \psi(U) \rangle}{\delta U^2}, \tag{S62}$$

where $L = 2 \times L_x$ is the total number of sites and $|\psi(U)\rangle$ denotes the ground-state matrix-product state.

For filling $\nu = 1$, the results are presented in the main text. Convergence was achieved using a maximum bond dimension $\chi_{\max} = 1800$ for $L_x = 40, 44, 48$, and $\chi_{\max} = 1600$ for $L_x = 32$. The singular-value decomposition cutoff was set to 10^{-10} for all system sizes, yielding an energy convergence better than 5×10^{-7} in all cases. The displacement in the interaction strength in Eq. (S62) was fixed to $\delta U = 0.002$.

We were unable to reliably identify the $\nu = 3/4$ transition within the present DMRG simulations, and a detailed study of this filling is left for future work, while the case $\nu = 1/2$ was already investigated in Ref. [52].

The $\nu = 1/4$ transition is discussed in the main text, while additional numerical results are presented in Fig. S4. Figs. S4(a) and (b) show the behavior of $\langle \hat{L} \rangle$ and the plaquette loop current correlator maybe C_p for different system lengths. Figure S4(c) displays the opening of the charge gap, defined as $\Delta E_c = E(N+1) - 2E(N) + E(N-1)$. The nature of the transition can be inferred from panel (c): the emergence of a finite ΔE_c indicates that the system becomes incompressible, signaling the onset of a Mott insulating phase. Concurrently, the finite loop current confirms the chiral character of the superfluid phase.

The effective theory developed in Ref. [52] shows that the low-energy physics of weakly interacting bosons in a π -flux plaquette shares important similarities with that of p -band bosons. However, crucial differences occur, one example is the transition at filling $\nu = 1/4$. Indeed, in p -band models the strong anisotropy of orbital hopping induce a transition into a non-chiral phase described by a classical product state theory [69, 70]. Here the situation changes

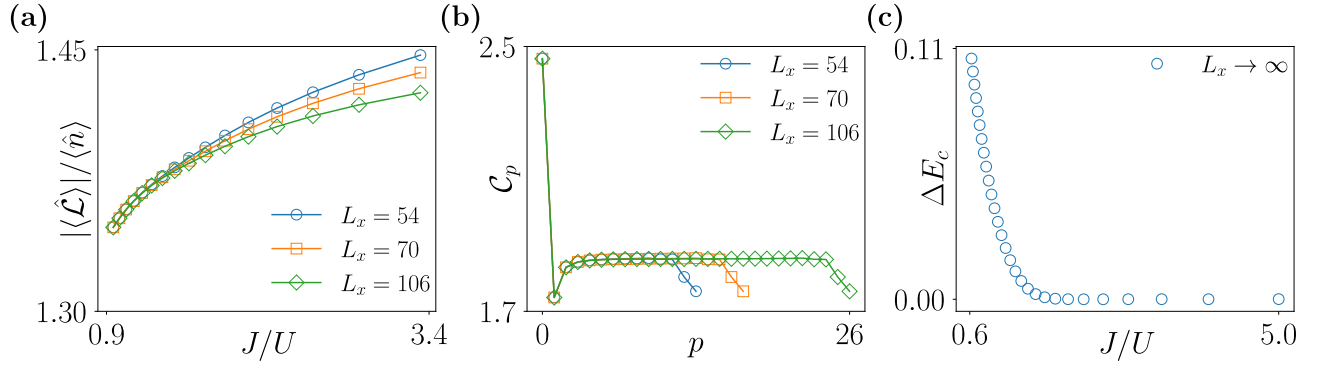


Figure S4. Additional DMRG results for $\nu = 1/4$ for $J = 0.1J'$. (a): $|\langle \hat{L} \rangle|/\langle \hat{n} \rangle$ for different ladder lengths $L = 54, 70, 106$. (c): Loop current-loop current correlation throughout all the transition. (c): Charge gap ΔE_c computed as the fit to $L \rightarrow \infty$ from the value of $L_x=70,98,106$.

as the emergent orbitals hop with the same strength in all spatial directions (J'). The Gutzwiller ansatz predicts a transition into a vortex-chiral Mott phase. To further substantiate the nature of this vortex phase, we employ a perturbative approach analogous to that used in Refs. [69, 70]. As stated in the main text, at second order in perturbation theory with $\hat{\sigma}_p^z$ corresponding to loop current states, one obtains

$$\hat{H}_{\text{eff}} = -\frac{5}{2} \frac{J'^2}{U} - \frac{J'^2}{U} \sum_{\langle p,q \rangle} \left[\frac{3}{4} \hat{\sigma}_p^z \hat{\sigma}_q^z + \frac{1}{4} (\hat{\sigma}_p^x \hat{\sigma}_q^x + \hat{\sigma}_p^y \hat{\sigma}_q^y) \right] \quad (\text{S63})$$

which suggests a chiral ferromagnetic ground state in this regime, explaining the chiral gapped order. Notice that differently from p -bands, not only the phase is chiral but also the it is described at leading order by a quantum theory and not a classical (Ising) model.